2002

Calculation of the stability index in parameter-dependent calculus of variations problems: Buckling of a twisted elastic strut

Kathleen A. Hoffman

Robert S. Manning
Haverford College, rmanning@haverford.edu

Randy C. Paffenroth

SIAM J. Applied Dynamical Systems
Vol. 1, No. 1, pp. 115–145

Calculation of the Stability Index in Parameter-Dependent Calculus of Variations Problems: Buckling of a Twisted Elastic Strut*

Kathleen A. Hoffman†, Robert S. Manning‡, and Randy C. Paffenroth§

Abstract. We consider the problem of minimizing the energy of an inextensible elastic strut with length 1 subject to an imposed twist angle and force. In a standard calculus of variations approach, one first locates equilibria by solving the Euler–Lagrange ODE with boundary conditions at arclength values 0 and 1. Then one classifies each equilibrium by counting conjugate points, with local minima corresponding to equilibria with no conjugate points. These conjugate points are arclength values $\sigma \leq 1$ at which a second ODE (the Jacobi equation) has a solution vanishing at 0 and σ.

Finding conjugate points normally involves the numerical solution of a set of initial value problems for the Jacobi equation. For problems involving a parameter λ, such as the force or twist angle in the elastic strut, this computation must be repeated for every value of λ of interest.

Here we present an alternative approach that takes advantage of the presence of a parameter λ. Rather than search for conjugate points $\sigma \leq 1$ at a fixed value of λ, we search for a set of special parameter values λ_m (with corresponding Jacobi solution $\boldsymbol{\zeta}^m$) for which $\sigma = 1$ is a conjugate point. We show that, under appropriate assumptions, the index of an equilibrium at *any* λ equals the number of these $\boldsymbol{\zeta}^m$ for which $\langle \boldsymbol{\zeta}^m, \mathcal{S}\boldsymbol{\zeta}^m \rangle < 0$, where $\mathcal{S}$ is the Jacobi differential operator at λ. This computation is particularly simple when λ appears linearly in $\mathcal{S}$.

We apply this approach to the elastic strut, in which the force appears linearly in $\mathcal{S}$, and, as a result, we locate the conjugate points for any twisted unbuckled rod configuration without resorting to numerical solution of differential equations. In addition, we numerically compute two-dimensional sheets of buckled equilibria (as the two parameters of force and twist are varied) via a coordinated family of one-dimensional parameter continuation computations. Conjugate points for these buckled equilibria are determined by numerical solution of the Jacobi ODE.

Key words. elastic rods, anisotropy, stability index, conjugate points, buckling, parameter continuation, isoperimetric constraints

AMS subject classifications. 49K15, 34B08, 74K10, 74G60, 65P30, 65L10

PII. S1111111101396622

1. Introduction.

The classification of equilibria is a familiar idea from finite-dimensional optimization. Given an equilibrium (or critical point) of a function, one computes the eigenvalues of the Hessian matrix and determines the type of the equilibrium by computing the index, the number of negative eigenvalues. Equilibria with index 0 are local minima, and those

*Received by the editors October 17, 2001; accepted for publication (in revised form) by P. Holmes May 6, 2002; published electronically July 23, 2002.

http://www.siam.org/journals/siads/1-1/39662.html

†Department of Mathematics and Statistics, University of Maryland, Baltimore County, MD 21250 (khoffman@math.umbc.edu).

‡Mathematics Department, Haverford College, Haverford, PA 19041 (rmanning@haverford.edu). The research of this author was supported by NSF grant DMS-9973258.

§Applied and Computational Mathematics, California Institute of Technology, Pasadena, CA 91125 (redrod@acm.org). The research of this author was supported by NSF grant KDI/NCC Molecular information and computer modeling in electrophysiology, SBR-9873173.

with index 1 are saddle points with one downward direction, etc. The goal is analogous in infinite dimensions, when the quantity J to be optimized is itself a function of a function $\mathbf{q}(s)$, say, with $0 \leq s \leq 1$.[1] Now the equilibria $\mathbf{q}_0(s)$ are found by solving the Euler–Lagrange ordinary differential equation (ODE). The role of the Hessian is played by the second-variation operator, and the notion of index, the number of negative eigenvalues in the spectrum of this operator, remains, with local minima again characterized as having index 0. In many applications, s is a spatial variable and J a potential energy,[2] and we think of the index as determining "stability," with the idea that, when time-dependence and a kinetic energy are added to this potential energy, the index-0 local minima will likely be dynamically stable. We emphasize, however, that, in this paper, "stability" is purely a classification of the type of equilibrium for an optimization problem.

In the calculus of variations, there is a powerful theory that allows a relatively simple determination of the index (see, e.g., [9]). Given an equilibrium, one consider the associated Jacobi equation, a linear second-order ODE. One then defines the notion of a conjugate point, which is a number σ, such that the Jacobi equation has a nonzero solution that vanishes at $s = 0$ and $s = \sigma$. Jacobi's strengthened condition says that the equilibrium is a local minimum if it has no conjugate point in $(0, 1]$. Morse [20] later generalized this theory to show that, assuming 1 is not a conjugate point, the number of conjugate points in $(0, 1)$ is the index of the equilibrium. This Euler–Jacobi–Morse index theory thus achieves a remarkable simplification: it reduces the problem of counting the number of negative eigenvalues of the second-variation operator of J in infinite-dimensional space to the problem of solving a second-order ODE and counting conjugate points. Thus the only numerical approximation arises in the discretization of ODEs, namely, the Euler–Lagrange and Jacobi equations.

Here we present a further simplification applicable to parameter-dependent problems and especially problems in which a parameter λ appears linearly in the second variation—for example, in problems containing a Lagrange multiplier. In this case, the counting of conjugate points at $\sigma \leq 1$ for a fixed value of λ can be reduced to the problem of analyzing conjugate points at the fixed value $\sigma = 1$ as λ is allowed to vary. Often, the determination of conjugate points at $\sigma = 1$ is easier than the general analysis of conjugate points for $\sigma \leq 1$, so this reduction can be a significant simplification. Of course, in cases where the relevant differential equations cannot be solved in closed form, this simplification is impractical, and one must revert to computing conjugate points numerically.

We further show that this entire theory can be carried through to the case of problems with isoperimetric constraints, where the only required change is an update to the definition of a conjugate point. This updated definition of a "constrained conjugate point" is the one taken, e.g., by Bolza [2] and rephrased in functional analytic language in Manning, Rogers,

[1] To rigorously define optimization in infinite dimensions, a normed space must be specified for the input functions $\mathbf{q}$. Following standard practice, we use the $C^1([0, 1])$ norm, in which case the resulting minima are traditionally referred to as "weak minima" [9].

[2] We note in passing an interesting exception. When J is a Lagrangian action functional and s represents time, the equilibria are classical mechanical trajectories, and the index plays a crucial role in the semiclassical approximation of these trajectories as quantum mechanical limits are approached [13]. The example in this paper involves a potential energy functional, but the general theory presented could equally well be applied to the determination of the semiclassical index for classical trajectories dependent on some parameter.

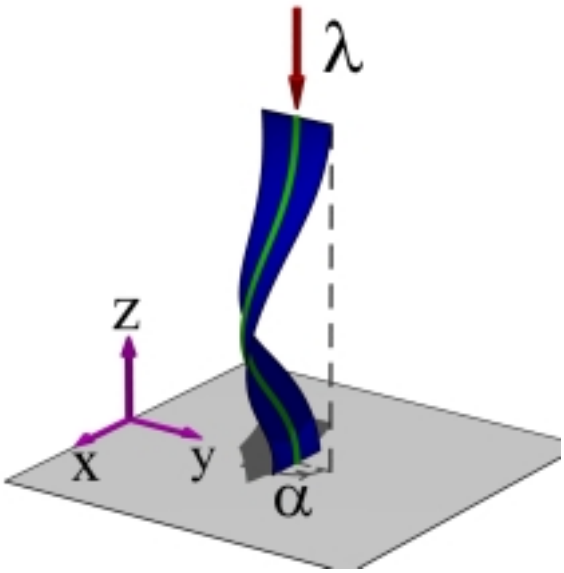

Figure 1.1. *An elastic strut clamped at each end, with a relative twist angle α, and with one end allowed to slide vertically in response to an imposed force λ. The cross-sections of the rod are elliptical, which we depict by showing the curve through the centers of the cross-sections as a green tube and tracking the major axes of the cross-sections with a blue ribbon.*

and Maddocks [19].

We apply this method for direct index computation to the example of a thin elastic strut with an elliptical (anisotropic) or circular (isotropic) cross-section, under the constraints shown in Figure 1.1. One end of the rod is clamped at the origin, with the major axis of the ellipse along the x-axis, the minor axis along the y-axis, and the tangent vector to the rod along the z-axis. The other end is constrained to lie along the z-axis, with its tangent vector also along the z-axis and its cross-section twisted by an angle α with respect to the x-y plane, but can slide up and down the z-axis in response to an applied vertical force λ.

Such a rod buckling problem has fed the curiosity of scientists since the time of Euler and Lagrange [17]. In 1883, Greenhill [11] considered the plane (over all values of α and λ) of unbuckled configurations for an isotropic strut and derived the condition for the index to be zero. More recently, Champneys and Thompson [3] and van der Heijden and Thompson [27] performed bifurcation analyses of an anisotropic elastic rod but did not focus on the question of stability. Goriely, Nizette, and Tabor [10] considered the dynamic stability of the unbuckled configurations for both the isotropic and anisotropic cases, and van der Heijden et al. [26] inferred stability for unbuckled and buckled configurations for the isotropic case from the shape of solution branches in a particular "distinguished" coordinate system. Neukirch and Henderson [21] performed an in-depth classification of buckled solutions for the isotropic problem, including the computation of two-dimensional sheets of equilibria.

Here we present stability results for this problem that both complement the results cited above and serve as an illustration for the general index theory we develop. Specifically, this theory allows a semianalytic determination of the index on the plane of unbuckled configura-

tions for both the isotropic and anisotropic strut. (The determination is semianalytic in that it requires the numerical solution of an algebraic equation but no differential equations.) In addition, we compute sheets of buckled solutions using a family of one-dimensional branches generated by the parameter continuation package AUTO [5, 6]. We determine the index of configurations on these sheets via a numerical implementation of the conjugate point test developed in [19] since a closed-form solution of the differential equations is not feasible in this case.

We begin in section 2 by reviewing conjugate point theory for unconstrained and constrained problems. Section 3 presents our direct method for computing the index for unconstrained problems, which is then extended to problems with isoperimetric constraints in section 4. In section 5, we summarize the standard Kirchhoff theory of inextensible and unshearable elastic struts. The index on the plane of unbuckled equilibria for both the isotropic and anisotropic strut is determined in section 6, and the buckled configurations and their stability are presented in section 7.

2. A review of conjugate point theory.

2.1. Unconstrained conjugate points. In this section, we summarize conjugate point theory for unconstrained calculus of variations problems. This theory is an established part of the classic unconstrained calculus of variations literature and can be found in many standard texts, e.g., [7, 9, 14, 24]. However, index theory appears only in more modern treatments [12, 20].

We consider a functional of the form

$$J[\mathbf{q}] = \int_0^1 L(\mathbf{q}, \mathbf{q}', s)\, ds, \quad \mathbf{q}(s) \in \mathbb{R}^p, \tag{2.1}$$
$$\text{subject to } \mathbf{q}(0) = \mathbf{h}_0, \quad \mathbf{q}(1) = \mathbf{h}_1.$$

Equilibria $\mathbf{q}_0(s)$ are solutions to the standard Euler–Lagrange equations for the functional J. Classification of these equilibria involves an analysis of the second variation of J at $\mathbf{q}_0$, namely,

$$\delta^2 J[\boldsymbol{\zeta}] = \frac{1}{2}\int_0^1 \left[(\boldsymbol{\zeta}')^T \mathbf{P}\boldsymbol{\zeta}' + (\boldsymbol{\zeta}')^T \mathbf{C}^T\boldsymbol{\zeta} + \boldsymbol{\zeta}^T\mathbf{C}\boldsymbol{\zeta}' + \boldsymbol{\zeta}^T\mathbf{Q}\boldsymbol{\zeta}\right] ds \tag{2.2}$$

for $\mathbf{P} \equiv L^0_{\mathbf{q}'\mathbf{q}'}$, $\mathbf{C} \equiv L^0_{\mathbf{q}\mathbf{q}'}$, and $\mathbf{Q} \equiv L^0_{\mathbf{q}\mathbf{q}}$, where, here and throughout, superscripting by T denotes the transpose, subscripting by $\mathbf{q}$ or $\mathbf{q}'$ denotes partial differentiation, and superscripting by 0 denotes evaluation at $\mathbf{q}_0(s)$. We assume that Legendre's strengthened condition holds,

$$\mathbf{P} > 0; \tag{2.3}$$

i.e., the symmetric matrix $\mathbf{P}$ is positive definite. Here $\boldsymbol{\zeta}$ is a variation in $\mathbf{q}$ that, due to the boundary conditions on $\mathbf{q}$, must lie in the set of admissible variations:

$$\mathcal{H}_d \equiv \left\{\boldsymbol{\zeta} \in H^2(\mathbb{R}^p, (0,1)) : \boldsymbol{\zeta}(0) = \boldsymbol{\zeta}(1) = \mathbf{0}\right\}.$$

Here we have chosen the Sobolev space H^2 of functions with integrable weak second derivatives because, after an integration by parts, the second variation will take the form

$$\delta^2 J[\boldsymbol{\zeta}] = \frac{1}{2}\langle \boldsymbol{\zeta}, \mathcal{S}\boldsymbol{\zeta}\rangle,$$

where $\mathcal{S}$ is the self-adjoint second-order vector differential operator

$$\mathcal{S}\boldsymbol{\zeta} \equiv -\frac{d}{ds}\left[\mathbf{P}\boldsymbol{\zeta}' + \mathbf{C}^T\boldsymbol{\zeta}\right] + \mathbf{C}\boldsymbol{\zeta}' + \mathbf{Q}\boldsymbol{\zeta}, \tag{2.4}$$

and $\langle\cdot,\cdot\rangle$ denotes the usual inner product in $L^2(\mathbb{R}^p,(0,1))$:

$$\langle \mathbf{f}, \mathbf{g}\rangle = \int_0^1 [\mathbf{f}(s)]^T \mathbf{g}(s)\, ds.$$

A sufficient condition for $\mathbf{q}_0$ to be a local minimum of J is a combination of Legendre's strengthened condition (2.3) with Jacobi's strengthened condition that $\mathbf{q}_0$ has no *conjugate point* in $(0,1]$, where a conjugate point is defined to be a value σ for which there is a nontrivial solution to

$$\mathcal{S}\boldsymbol{\zeta} = \mathbf{0}, \quad 0 < s < \sigma, \quad \boldsymbol{\zeta}(0) = \boldsymbol{\zeta}(\sigma) = \mathbf{0}. \tag{2.5}$$

Morse [20] extended Jacobi's condition to equate the number of conjugate points with the index that quantifies the dimension of the set on which $\delta^2 J$ is negative.

In some cases, (2.5) can be solved analytically, but generically a numerical procedure for computing conjugate points is required. For completeness, we briefly summarize a standard algorithm for computing unconstrained conjugate points [24, p. 152]. We numerically compute a basis of solutions $\{\boldsymbol{\zeta}_1,\ldots,\boldsymbol{\zeta}_p\}$ to the homogeneous second-order initial value problem

$$\mathcal{S}\boldsymbol{\zeta} = \mathbf{0}, \quad \boldsymbol{\zeta}(0) = \mathbf{0}. \tag{2.6}$$

A conjugate point occurs when a nontrivial linear combination of $\{\boldsymbol{\zeta}_1,\ldots,\boldsymbol{\zeta}_p\}$ vanishes, i.e., when there is a nontrivial solution to the $p\times p$ linear system

$$\begin{bmatrix}\boldsymbol{\zeta}_1 & \cdots & \boldsymbol{\zeta}_p\end{bmatrix}\begin{bmatrix}c_1\\ \vdots\\ c_p\end{bmatrix} = \mathbf{0}. \tag{2.7}$$

Therefore, as we build up solutions $\boldsymbol{\zeta}_j(\sigma)$ to (2.6) as σ grows from 0 to 1, we track the determinant of the $p\times p$ matrix $\begin{bmatrix}\boldsymbol{\zeta}_1(\sigma) & \cdots & \boldsymbol{\zeta}_p(\sigma)\end{bmatrix}$ and count as a conjugate point every time this determinant crosses zero.

2.2. Constrained conjugate points. In this section, we review a definition of a conjugate point appropriate for calculus of variations problems with isoperimetric constraints:

$$\begin{aligned} W[\mathbf{q}] &= \int_0^1 L(\mathbf{q},\mathbf{q}',s)\, ds, \quad \mathbf{q}(s)\in\mathbb{R}^p,\\ \text{subject to } &\int_0^1 g_i(\mathbf{q})\, ds = 0, \quad i=1,\ldots,n,\\ &\mathbf{q}(0)=\mathbf{h}_0, \quad \mathbf{q}(1)=\mathbf{h}_1. \end{aligned}$$

According to the usual multiplier rule, an associated functional

$$J[\mathbf{q}] = \int_0^1 \left(L + \mathbf{g}^T \boldsymbol{\nu}\right)\, ds$$

is constructed, and constrained equilibria $(\mathbf{q}_0(s), \boldsymbol{\nu}_0)$ of W are solutions of the standard unconstrained Euler–Lagrange equations for the functional J, with the multiplier $\boldsymbol{\nu}_0$ determined by the integral constraints. The second variation $\delta^2 J$ and its associated operator $\mathcal{S}$ take the unconstrained forms (2.2) and (2.4) but now with $\mathbf{Q} = [\mathbf{g}^0_{\mathbf{qq}}]^T \boldsymbol{\nu}_0 + L^0_{\mathbf{qq}}$. Admissible variations $\boldsymbol{\zeta}$ must satisfy the linearized constraints

$$\langle \boldsymbol{\zeta}, \mathbf{T}_i \rangle = 0, \quad i = 1, \ldots, n,$$

where

$$\mathbf{T}_i \equiv (g_i)^0_{\mathbf{q}}.$$

We assume that the $\mathbf{T}_i(s)$ are linearly independent on $(0, \sigma)$ for each $\sigma \in (0, 1]$. So the admissible set of constrained variations is

$$\mathcal{H}_d^{cons} \equiv \{\boldsymbol{\zeta} \in \mathcal{H}_d : \langle \boldsymbol{\zeta}, \mathbf{T}_i \rangle = 0, \;\; i = 1, \ldots, n\}.$$

Bolza [2], citing the work of Weierstrass and Kneser, defined the relevant notion of conjugate point for an isoperimetric problem, namely, that σ is called a conjugate point if the following system has a nontrivial solution:

$$\begin{aligned} &\mathcal{S}\boldsymbol{\zeta} = \sum_{i=1}^{n} \breve{c}_i \mathbf{T}_i, \quad 0 < s < \sigma, \;\; \text{for some constants } \breve{c}_i, \\ &\boldsymbol{\zeta}(0) = \boldsymbol{\zeta}(\sigma) = \mathbf{0}, \qquad \int_0^\sigma \boldsymbol{\zeta}^T \mathbf{T}_i \, ds = 0, \;\; i = 1, \ldots, n. \end{aligned} \tag{2.8}$$

In [19], we introduced an orthogonal projection operator $\mathcal{Q}$ onto the L^2-orthogonal complement of $\operatorname{span}(\mathbf{T}_1, \ldots, \mathbf{T}_n)$ to rewrite Bolza's conjugate point condition (2.8) in the equivalent form

$$\begin{aligned} &(\mathcal{Q}\mathcal{S}\mathcal{Q})\boldsymbol{\zeta} = \mathbf{0}, \quad 0 < s < \sigma, \\ &\boldsymbol{\zeta}(0) = \boldsymbol{\zeta}(\sigma) = \mathbf{0}, \qquad \int_0^\sigma \boldsymbol{\zeta}^T \mathbf{T}_i \, ds = 0, \;\; i = 1, \ldots, n. \end{aligned} \tag{2.9}$$

Further, the arguments in [19], involving a proof of the monotonicity of the eigenvalues of $\mathcal{Q}\mathcal{S}\mathcal{Q}$ as a function of σ, demonstrate the analogue to Jacobi's strengthened condition: the lack of an isoperimetric conjugate point implies the existence of a local minimum. In addition, similar to Morse's theory in the unconstrained case, the number of isoperimetric conjugate points equals the maximal dimension of a subspace of $\mathcal{H}_d^{cons}$ on which the second variation is negative.

There is also a technique for the numerical determination of these conjugate points similar to the procedure described in section 2.1 for the unconstrained case. We summarize this

technique here and refer the interested reader to [19] for complete details. In addition to numerically determining a basis of solutions to (2.6), we also compute solutions $\breve{\boldsymbol{\zeta}}_i$ to each of the n nonhomogeneous initial value problems

$$\mathcal{S}\boldsymbol{\zeta} = \mathbf{T}_i, \quad \boldsymbol{\zeta}(0) = \mathbf{0}.$$

A conjugate point occurs when there exists a nontrivial linear combination of $\{\boldsymbol{\zeta}_1, \dots, \boldsymbol{\zeta}_p, \breve{\boldsymbol{\zeta}}_1, \dots \breve{\boldsymbol{\zeta}}_n\}$ that vanishes and also obeys the linearized constraints $\int_0^\sigma \boldsymbol{\zeta}^T \mathbf{T}_i ds = 0$. This condition has a $(p+n)$-by-$(p+n)$ matrix form analogous to the p-by-p unconstrained matrix equation (2.7). As in the unconstrained case, the matrix entries are built up by solving initial value problems as σ grows from 0 to 1, and the conjugate points are found by zero-crossings of the $(p+n)$-by-$(p+n)$ determinant.

3. Analytic determination of the index for unconstrained parameter-dependent problems. In this section, we describe an alternative approach to determining the index for equilibria of (2.1) when L, and hence the second-variation operator $\mathcal{S}$, depends on a parameter λ. This approach allows, in some cases, an analytic determination of the index. The key idea is to relate the index at a *specific* value of the parameter λ to the set of all parameter values λ that yield conjugate points at $\sigma = 1$, i.e., solutions of

$$\mathcal{S}(\lambda)\boldsymbol{\zeta} = \mathbf{0}, \quad \boldsymbol{\zeta}(0) = \boldsymbol{\zeta}(1) = \mathbf{0}. \tag{3.1}$$

We will denote solutions to (3.1) by $(\lambda_m, \boldsymbol{\zeta}^m)$ and refer to λ_m as *branch points*. This name is appropriate since, in all cases we consider, new branches of equilibria will arise at λ_m. In many applications, the analytic determination of $(\lambda_m, \boldsymbol{\zeta}^m)$ is possible even when the general conjugate point equation (2.5) cannot be solved in closed form.

We will assume that $\{\boldsymbol{\zeta}^m\}$ form a basis for $\mathcal{H}_d$ and that they are $\mathcal{S}$-orthogonal, i.e., that $\langle \boldsymbol{\zeta}^m, \mathcal{S}\boldsymbol{\zeta}^n \rangle = 0$ for all $m \neq n$. These assumptions hold for many physically motivated problems, including cases in which (3.1) is a standard Sturm–Liouville eigenvalue problem (see, e.g., [23, p. 273]). This basis of solutions can then be used to diagonalize $\mathcal{S}$ and determine the index directly, as shown by the following lemma.

Lemma 3.1. *Assume that $\{\boldsymbol{\zeta}^m\}$ form an $\mathcal{S}$-orthogonal basis of $\mathcal{H}_d$. Then the index equals the number of $\boldsymbol{\zeta}^m$ for which $\langle \boldsymbol{\zeta}^m, \mathcal{S}\boldsymbol{\zeta}^m \rangle < 0$.*

Proof. Let $\mathcal{N}$ be the subspace of $\mathcal{H}_d$ spanned by those $\boldsymbol{\zeta}^m$ for which $\langle \boldsymbol{\zeta}^m, \mathcal{S}\boldsymbol{\zeta}^m \rangle < 0$. Any $\boldsymbol{\chi} \in \mathcal{H}_d$ that is L^2-orthogonal to $\mathcal{N}$ can be written as

$$\boldsymbol{\chi} = \sum_{\boldsymbol{\zeta}^m \notin \mathcal{N}} c_m \boldsymbol{\zeta}^m,$$

where the notation $\sum_{\boldsymbol{\zeta}^m \notin \mathcal{N}}$ denotes a sum over all m for which $\boldsymbol{\zeta}^m \notin \mathcal{N}$. Then, by $\mathcal{S}$-orthogonality,

$$\langle \boldsymbol{\chi}, \mathcal{S}\boldsymbol{\chi} \rangle = \sum_{\boldsymbol{\zeta}^m \notin \mathcal{N}} (c_m)^2 \langle \boldsymbol{\zeta}^m, \mathcal{S}\boldsymbol{\zeta}^m \rangle.$$

By definition, $\langle \boldsymbol{\zeta}^m, \mathcal{S}\boldsymbol{\zeta}^m \rangle \geq 0$ for all terms in the sum, so $\langle \boldsymbol{\chi}, \mathcal{S}\boldsymbol{\chi} \rangle \geq 0$.

Table 3.1
Index for the planar Euler buckling problem.

Range of λ	Functions $\boldsymbol{\zeta}^m$ for which $\langle \boldsymbol{\zeta}^m, \mathcal{S}(\lambda)\boldsymbol{\zeta}^m \rangle < 0$	Index
$0 < \lambda < \pi^2$	none	0
$\pi^2 < \lambda < 4\pi^2$	ζ^1	1
$4\pi^2 < \lambda < 9\pi^2$	ζ^1, ζ^2	2
$9\pi^2 < \lambda < 16\pi^2$	$\zeta^1, \zeta^2, \zeta^3$	3

Thus $\mathcal{N}$ is a maximal subspace in $\mathcal{H}_d$ on which the second variation is negative. The index is defined to be the dimension of $\mathcal{N}$, which, by definition of $\mathcal{N}$, is the number of basis functions $\boldsymbol{\zeta}^m$ for which $\langle \boldsymbol{\zeta}^m, \mathcal{S}\boldsymbol{\zeta}^m \rangle < 0$. ■

The above diagonalization is particularly useful when the parameter λ appears linearly in $\mathcal{S}$,

$$\mathcal{S}\boldsymbol{\zeta} = \mathcal{S}_1\boldsymbol{\zeta} + \lambda\mathcal{S}_2\boldsymbol{\zeta}, \tag{3.2}$$

because it is then routine to determine those basis functions $\boldsymbol{\zeta}^m$ for which $\langle \boldsymbol{\zeta}^m, \mathcal{S}\boldsymbol{\zeta}^m \rangle < 0$. In fact, the quantity $\langle \boldsymbol{\zeta}^m, \mathcal{S}\boldsymbol{\zeta}^m \rangle$ is simply related to the λ-independent quantity $\langle \boldsymbol{\zeta}^m, \mathcal{S}_2\boldsymbol{\zeta}^m \rangle$ by the following lemma.

Lemma 3.2. *Suppose $\mathcal{S}$ takes the form (3.2). Then, for any solution $(\lambda_m, \boldsymbol{\zeta}^m)$ of (3.1),*

$$\langle \boldsymbol{\zeta}^m, \mathcal{S}\boldsymbol{\zeta}^m \rangle = (\lambda - \lambda_m)\langle \boldsymbol{\zeta}^m, \mathcal{S}_2\boldsymbol{\zeta}^m \rangle.$$

Proof. The key idea is to exploit the fact that $(\mathcal{S}_1 + \lambda_m\mathcal{S}_2)\boldsymbol{\zeta}^m = \mathbf{0}$:

$$\begin{aligned}\langle \boldsymbol{\zeta}^m, \mathcal{S}\boldsymbol{\zeta}^m \rangle &= \langle \boldsymbol{\zeta}^m, (\mathcal{S}_1 + \lambda\mathcal{S}_2)\boldsymbol{\zeta}^m \rangle \\ &= \langle \boldsymbol{\zeta}^m, (\mathcal{S}_1 + \lambda_m\mathcal{S}_2 - \lambda_m\mathcal{S}_2 + \lambda\mathcal{S}_2)\boldsymbol{\zeta}^m \rangle = (\lambda - \lambda_m)\langle \boldsymbol{\zeta}^m, \mathcal{S}_2\boldsymbol{\zeta}^m \rangle.\end{aligned}$$ ■

Lemmas 3.1 and 3.2 lead immediately to the following corollary, the central result of this article.

Corollary 3.3. *If the solutions of (3.1) form an $\mathcal{S}$-orthogonal basis for $\mathcal{H}_d$ and if $\mathcal{S}$ has the form (3.2), then the index of an equilibrium at parameter value λ equals the number of branch points λ_m such that $\lambda > \lambda_m$ and $\langle \boldsymbol{\zeta}^m, \mathcal{S}_2\boldsymbol{\zeta}^m \rangle < 0$, plus the number of branch points λ_m such that $\lambda < \lambda_m$ and $\langle \boldsymbol{\zeta}^m, \mathcal{S}_2\boldsymbol{\zeta}^m \rangle > 0$.*

Example (planar buckling of a strut). We parametrize the strut by arclength s and choose a length scale so that $0 \le s \le 1$. We let $\theta(s)$ denote the angle that the strut makes with vertical at position s. We impose the boundary conditions that the strut be vertical at $s = 0$ and $s = 1$ and impose a vertical force λ. We then have the calculus of variations problem to minimize the total energy

$$\int_0^1 \left[\frac{1}{2}K(\theta'(s))^2 + \lambda\cos(\theta(s))\right] ds, \quad \theta(0) = \theta(1) = 0,$$

where $K > 0$ is a stiffness parameter.

Consider the unbuckled equilibrium $\theta(s) = 0$. The second-variation operator is $\mathcal{S}\zeta = -K\zeta'' - \lambda\zeta$, which is of the form (3.2), with $\mathcal{S}_2 = -1$. The nontrivial solutions to (3.1) are $\zeta^m(s) = A\sin(m\pi s)$, $m = 1, 2, 3, \ldots$, with $\lambda_m = m^2\pi^2$. These solutions are an $\mathcal{S}$-orthogonal basis for $\mathcal{H}_d$ since $\mathcal{S}$ is a Sturm–Liouville operator. We observe that $\langle \zeta^m, \mathcal{S}_2\zeta^m\rangle < 0$ for all m and then use Lemma 3.2 to conclude that the sign of $\langle \zeta^m, \mathcal{S}(\lambda)\zeta^m\rangle$ is the same as the sign of $m^2\pi^2 - \lambda$. Hence we conclude that the index for arbitrary λ is as given in Table 3.1.

4. Analytic determination of the index for isoperimetrically constrained parameter-dependent problems. Next we combine the ideas of the previous two sections to produce a method for directly computing the index in a calculus of variations problem with isoperimetric constraints, when the second-variation operator $\mathcal{S}$ depends on a parameter λ. As in section 3, we assume that solutions $\boldsymbol{\zeta}^m$ of

$$\begin{aligned} &\mathcal{S}(\lambda)\boldsymbol{\zeta} = \sum_{i=1}^{n} \breve{c}_i \mathbf{T}_i, \quad 0 < s < 1, \quad \text{for some constants } \breve{c}_i, \\ &\boldsymbol{\zeta}(0) = \boldsymbol{\zeta}(1) = \mathbf{0}, \qquad \int_0^1 \boldsymbol{\zeta}^T \mathbf{T}_i \, ds = 0, \quad i = 1, \ldots, n, \end{aligned} \tag{4.1}$$

form an $\mathcal{S}$-orthogonal basis for the relevant function space $\mathcal{H}_d^{cons}$. Although (4.1) reflects Bolza's definition of conjugate point at $\sigma = 1$, we will exploit the equivalence of (2.8) and (2.9) to rewrite the differential equation $\mathcal{S}(\lambda)\boldsymbol{\zeta} = \sum_{i=1}^n \breve{c}_i \mathbf{T}_i$ as $(\mathcal{Q}\mathcal{S}(\lambda)\mathcal{Q})\boldsymbol{\zeta} = \mathbf{0}$. As before, the basis $\{\boldsymbol{\zeta}^m\}$ will be used to diagonalize the projected operator $\mathcal{Q}\mathcal{S}\mathcal{Q}$ on $\mathcal{H}_d^{cons}$. In fact, Lemma 3.1 holds for the constrained case, provided $\mathcal{H}_d$ is replaced with the space $\mathcal{H}_d^{cons}$, noting that, since $\mathcal{Q}$ is self-adjoint, $\langle \boldsymbol{\zeta}, (\mathcal{Q}\mathcal{S}\mathcal{Q})\boldsymbol{\zeta}\rangle = \langle \boldsymbol{\zeta}, \mathcal{S}\boldsymbol{\zeta}\rangle$ for $\boldsymbol{\zeta} \in \mathcal{H}_d^{cons}$.

If, in addition, $\mathcal{S}$ takes the form (3.2), then Lemma 3.2 can be extended to problems with isoperimetric constraints as follows.

Lemma 4.1. *Suppose $\mathcal{S}$ takes the form (3.2). Then, for any solution $\boldsymbol{\zeta}^m$ of (4.1),*

$$\langle \boldsymbol{\zeta}^m, (\mathcal{Q}\mathcal{S}\mathcal{Q})\boldsymbol{\zeta}^m\rangle = (\lambda - \lambda_m)\langle \boldsymbol{\zeta}^m, \mathcal{S}_2\boldsymbol{\zeta}^m\rangle.$$

Proof. As in Lemma 3.2, the key idea is to exploit the fact that $(\mathcal{Q}(\mathcal{S}_1 + \lambda_m\mathcal{S}_2)\mathcal{Q})\boldsymbol{\zeta}^m = \mathbf{0}$, combined with the fact that $\mathcal{Q}\boldsymbol{\zeta}^m = \boldsymbol{\zeta}^m$ for $\boldsymbol{\zeta}^m \in \mathcal{H}_d^{cons}$:

$$\begin{aligned} \langle \boldsymbol{\zeta}^m, (\mathcal{Q}\mathcal{S}\mathcal{Q})\boldsymbol{\zeta}^m\rangle &= \langle \boldsymbol{\zeta}^m, (\mathcal{Q}(\mathcal{S}_1 + \lambda\mathcal{S}_2)\mathcal{Q})\boldsymbol{\zeta}^m\rangle \\ &= \langle \boldsymbol{\zeta}^m, (\mathcal{Q}(\mathcal{S}_1 + \lambda_m\mathcal{S}_2 - \lambda_m\mathcal{S}_2 + \lambda\mathcal{S}_2)\mathcal{Q})\boldsymbol{\zeta}^m\rangle \\ &= \langle \mathcal{Q}\boldsymbol{\zeta}^m, (-\lambda_m\mathcal{S}_2 + \lambda\mathcal{S}_2)\mathcal{Q}\boldsymbol{\zeta}^m\rangle \\ &= (\lambda - \lambda_m)\langle \boldsymbol{\zeta}^m, \mathcal{S}_2\boldsymbol{\zeta}^m\rangle. \qquad \blacksquare \end{aligned}$$

Thus the strategy for analytically determining the index in problems with isoperimetric constraints is the same as for unconstrained problems. This strategy will be illustrated in section 6 for the example of the buckling of an elastic strut under imposed force and twist. In preparation for this example, we next summarize the basic elastic strut equations.

5. The elastic strut.

5.1. Equilibrium equations. In the Kirchhoff theory of inextensible and unshearable elastic struts [1, 4, 16, 17], the configuration of a strut is described by a centerline $\mathbf{r}(s)$ (written as a function of arclength s) and a set of directors $\{\mathbf{d}_1(s), \mathbf{d}_2(s), \mathbf{d}_3(s)\}$ that form an orthonormal frame giving the orientation of the cross-section of the strut. For convenience, we choose a length scale so that $0 \leq s \leq 1$. Let the superscript $'$ denote a derivative with respect to s. The assumptions of inextensibility and unshearability of the strut are incorporated in the requirement that $\mathbf{d}_3(s)$, the director orthogonal to the strut cross-section, equals $\mathbf{r}'(s)$, the tangent vector to the centerline.

Orthonormality of the directors implies the existence of a (Darboux) vector $\mathbf{u}(s)$ defined by the kinematic relations

$$\mathbf{d}_i'(s) = \mathbf{u}(s) \times \mathbf{d}_i(s), \quad i = 1, 2, 3.$$

The components of $\mathbf{u}$ in the strut frame are denoted by $u_i(s) = \mathbf{u}(s) \cdot \mathbf{d}_i(s)$ and are called the *strains*.

It will be convenient to describe the directors via Euler parameters or quaternions $\mathbf{q} \in \mathbb{R}^4$. Quaternions provide an alternate formulation to Euler angles for parametrizing rotation matrices in $SO(3)$ (see, e.g., [25, p. 462]). The directors $\mathbf{d}_i$ are the columns of a rotation matrix and can be expressed by rational functions of the quaternions,

$$\mathbf{d}_1 = \frac{1}{|\mathbf{q}|^2}\begin{bmatrix} q_1^2 - q_2^2 - q_3^2 + q_4^2 \\ 2q_1q_2 + 2q_3q_4 \\ 2q_1q_3 - 2q_2q_4 \end{bmatrix}, \quad \mathbf{d}_2 = \frac{1}{|\mathbf{q}|^2}\begin{bmatrix} 2q_1q_2 - 2q_3q_4 \\ -q_1^2 + q_2^2 - q_3^2 + q_4^2 \\ 2q_2q_3 + 2q_1q_4 \end{bmatrix},$$
$$\mathbf{d}_3 = \frac{1}{|\mathbf{q}|^2}\begin{bmatrix} 2q_1q_3 + 2q_2q_4 \\ 2q_2q_3 - 2q_1q_4 \\ -q_1^2 - q_2^2 + q_3^2 + q_4^2 \end{bmatrix},$$

and therefore the strains can be expressed as

$$u_1 = \frac{2}{|\mathbf{q}|^2}\left(q_1'q_4 + q_2'q_3 - q_3'q_2 - q_4'q_1\right), \quad u_2 = \frac{2}{|\mathbf{q}|^2}\left(-q_1'q_3 + q_2'q_4 + q_3'q_1 - q_4'q_2\right),$$
$$u_3 = \frac{2}{|\mathbf{q}|^2}\left(q_1'q_2 - q_2'q_1 + q_3'q_4 - q_4'q_3\right).$$

For convenience, we define $d_{3i}(s)$ to be the ith component of the vector $\mathbf{d}_3$. We impose the following constraints on the elastic strut:

(5.1)
$$\int_0^1 d_{31}(\mathbf{q}(s))\, ds = \int_0^1 d_{32}(\mathbf{q}(s))ds = 0, \quad \mathbf{q}(0) = (0,0,0,1), \quad \mathbf{q}(1) = (0,0,\sin(\alpha/2),\cos(\alpha/2)).$$

The boundary condition on $\mathbf{q}(0)$ forces the $s = 0$ end of the strut to be tangent to the z-axis. The pair of integral constraints imply, due to the inextensibility-unshearability condition $\mathbf{r}'(s) = \mathbf{d}_3(s)$, that $x(0) = x(1)$ and $y(0) = y(1)$, i.e., that the $s = 1$ end of the strut lies directly

above the $s = 0$ end. Finally, the boundary condition on $\mathbf{q}(1)$ implies that the $s = 1$ end of the strut is tangent to the z-axis and is twisted by an angle α with respect to the $s = 0$ end. Figure 1.1 depicts a solution that satisfies (5.1).

The elastic energy of the strut is expressed in terms of the strains, and we assume here a commonly used quadratic energy

$$E[\mathbf{q}] \equiv \int_0^1 \left[\sum_{i=1}^{3} \frac{1}{2} K_i \left[u_i(\mathbf{q}(s), \mathbf{q}'(s)) \right]^2 + \lambda d_{33} \right] ds,$$

where K_i are the bending ($i = 1, 2$) and twisting ($i = 3$) stiffnesses of the strut, and λ is a force pushing downward on the strut. Unbuckled twisted equilibria are described by

$$\mathbf{q}_0(s) = \begin{bmatrix} 0 \\ 0 \\ \sin(\frac{\alpha s}{2}) \\ \cos(\frac{\alpha s}{2}) \end{bmatrix},$$

which correspond to directors

$$\mathbf{d}_1 = \begin{bmatrix} \cos(\alpha s) \\ \sin(\alpha s) \\ 0 \end{bmatrix}, \quad \mathbf{d}_2 = \begin{bmatrix} -\sin(\alpha s) \\ \cos(\alpha s) \\ 0 \end{bmatrix}, \quad \mathbf{d}_3 = \begin{bmatrix} 0 \\ 0 \\ 1 \end{bmatrix}.$$

These are readily verified to be solutions to the Euler–Lagrange equations of the functional E. The goal of section 6 is to use the theory of section 4 to assign to these configurations a stability index.

5.2. The second variation. In this section, we show a routine but technical computation of the second variation of E, finding in the end that it takes the form $\mathcal{S} = \mathcal{S}_1 + \lambda \mathcal{S}_2$ required for our results. The computation is somewhat involved due to our choice to parametrize $SO(3)$ by four-dimensional quaternions.

As outlined in section 2.2, for each equilibrium $\mathbf{q}_0$, we define an *allowed variation* to be any $\delta\mathbf{q}$ so that $\delta\mathbf{q}(0) = \delta\mathbf{q}(1) = \mathbf{0}$ and $\langle \delta\mathbf{q}, (d_{3i})^0_{\mathbf{q}} \rangle = 0$ for $i = 1, 2$. The second variation of E is

$$\delta^2 E[\delta\mathbf{q}] = \int_0^1 \left[(\delta\mathbf{q}')^T L^0_{\mathbf{q}'\mathbf{q}'} \delta\mathbf{q}' + (\delta\mathbf{q}')^T L^0_{\mathbf{q}'\mathbf{q}} \delta\mathbf{q} + (\delta\mathbf{q})^T L^0_{\mathbf{q}\mathbf{q}'} \delta\mathbf{q}' + (\delta\mathbf{q})^T L^0_{\mathbf{q}\mathbf{q}} \delta\mathbf{q} \right] ds, \tag{5.2}$$

where L is the integrand of E with the appropriate Lagrange multiplier terms added to it.

We note first a property of $\delta^2 E$ peculiar to the example at hand. The integrand L is invariant to a scaling of $\mathbf{q}$, i.e.,

$$L(c\mathbf{q}, c\mathbf{q}') = L(\mathbf{q}, \mathbf{q}')$$

for any $c \in \mathbb{R}$. This degeneracy arises from our use of four-dimensional quaternions to represent the three-dimensional space $SO(3)$ of directors. If we write $\delta\mathbf{q}(s)$ as $\beta(s)\mathbf{q}_0(s) + \mathbf{w}(s)$, where, at each s, $\mathbf{w}(s)$ is perpendicular to $\mathbf{q}_0(s)$, then

$$E[\mathbf{q}_0 + \epsilon\delta\mathbf{q}] = E[(1 + \epsilon\beta)\mathbf{q}_0 + \epsilon\mathbf{w}] = E\left[\mathbf{q}_0 + \frac{\epsilon}{1 + \epsilon\beta} \mathbf{w} \right].$$

Therefore, $E[\mathbf{q}_0 + \epsilon\delta\mathbf{q}] < E[\mathbf{q}_0]$ for ϵ sufficiently small if and only if $E[\mathbf{q}_0 + \epsilon\mathbf{w}] < E[\mathbf{q}_0]$ for ϵ sufficiently small. Thus it is sufficient to consider only those allowed variations $\delta\mathbf{q}$ that are orthogonal to $\mathbf{q}_0$ at each s. For example, if we define a projection matrix $\mathbf{\Pi}(s) \in \mathbb{R}^{4\times 3}$ whose columns span the orthogonal complement of $\mathbf{q}_0(s)$, then an arbitrary $\delta\mathbf{q}(s)$ can be written as $\mathbf{\Pi}(s)\boldsymbol{\zeta}(s) + \beta(s)\mathbf{q}_0(s)$ for some $\boldsymbol{\zeta}(s) \in \mathbb{R}^3$ and $\beta(s) \in \mathbb{R}$, and the second variation we will need to consider is $\delta^2 E[\mathbf{\Pi}\boldsymbol{\zeta}]$. Thus we seek the maximal dimension of a subspace of functions $\boldsymbol{\zeta}(s) \in \mathbb{R}^3$ obeying $\delta^2 E[\mathbf{\Pi}\boldsymbol{\zeta}] < 0$, $\boldsymbol{\zeta}(0) = \boldsymbol{\zeta}(1) = \mathbf{0}$, and $\langle \mathbf{\Pi}\boldsymbol{\zeta}, (d_{3i})^0_{\mathbf{q}}\rangle = 0$ for $i = 1, 2$. For convenience, we observe that the constraints $\langle \mathbf{\Pi}\boldsymbol{\zeta}, (d_{3i})^0_{\mathbf{q}}\rangle = 0$ may be rewritten as $\langle \boldsymbol{\zeta}, \mathbf{T}_i\rangle = 0$ if we define $\mathbf{T}_i \equiv \mathbf{\Pi}^T (d_{3i})^0_{\mathbf{q}}$. The matrix $\mathbf{\Pi}$ will be defined differently for the anisotropic and the isotropic cases in sections 6.1 and 6.2, respectively.

Inserting $\delta\mathbf{q} = \mathbf{\Pi}\boldsymbol{\zeta}$ into (5.2) and integrating by parts terms starting with $(\boldsymbol{\zeta}')^T$, we find

$$\delta^2 J[\mathbf{\Pi}\boldsymbol{\zeta}] = \langle \boldsymbol{\zeta}, \mathcal{S}\boldsymbol{\zeta}\rangle,$$

where $\mathcal{S}$ is the operator

$$\mathcal{S}\boldsymbol{\zeta} = -\bar{\mathbf{P}}\boldsymbol{\zeta}'' + \bar{\mathbf{C}}\boldsymbol{\zeta}' + \bar{\mathbf{Q}}\boldsymbol{\zeta}$$

with coefficient matrices

$$\begin{aligned}
\bar{\mathbf{P}} &= \mathbf{\Pi}^T L^0_{\mathbf{q}'\mathbf{q}'}\mathbf{\Pi},\\
\bar{\mathbf{C}} &= (\mathbf{\Pi}')^T L^0_{\mathbf{q}'\mathbf{q}'}\mathbf{\Pi} + \mathbf{\Pi}^T L^0_{\mathbf{q}\mathbf{q}'}\mathbf{\Pi} - \left(\mathbf{\Pi}^T L^0_{\mathbf{q}'\mathbf{q}'}\mathbf{\Pi}' + \mathbf{\Pi}^T L^0_{\mathbf{q}'\mathbf{q}}\mathbf{\Pi}\right) - \left(\mathbf{\Pi}^T L^0_{\mathbf{q}'\mathbf{q}'}\mathbf{\Pi}\right)',\\
\bar{\mathbf{Q}} &= (\mathbf{\Pi}')^T L^0_{\mathbf{q}'\mathbf{q}'}\mathbf{\Pi}' + \mathbf{\Pi}^T L^0_{\mathbf{q}\mathbf{q}}\mathbf{\Pi} + \mathbf{\Pi}^T L^0_{\mathbf{q}\mathbf{q}'}\mathbf{\Pi}' + (\mathbf{\Pi}')^T L^0_{\mathbf{q}'\mathbf{q}}\mathbf{\Pi} - \left(\mathbf{\Pi}^T L^0_{\mathbf{q}'\mathbf{q}'}\mathbf{\Pi}' + \mathbf{\Pi}^T L^0_{\mathbf{q}'\mathbf{q}}\mathbf{\Pi}\right)'.
\end{aligned}$$

Our choices of $\mathbf{\Pi}$ will cause the last term in each of $\bar{\mathbf{C}}$ and $\bar{\mathbf{Q}}$ to vanish and will yield simple s-independent expressions for $\bar{\mathbf{P}}$, $\bar{\mathbf{C}}$, and $\bar{\mathbf{Q}}$. The resulting expression for $\mathcal{S}$ will take the form required by Lemma 3.2:

$$\mathcal{S} = \mathcal{S}_1 + \lambda\mathcal{S}_2.$$

Explicit forms for $\mathcal{S}_1$ and $\mathcal{S}_2$ depend on the choice of $\mathbf{\Pi}$ and so will be shown individually in sections 6.1 and 6.2.

6. Stability of unbuckled configurations.

6.1. The anisotropic strut.

For the anisotropic strut, we choose

$$\mathbf{\Pi}(s) \equiv \begin{bmatrix} \cos(\frac{\alpha s}{2}) & -\sin(\frac{\alpha s}{2}) & 0\\ \sin(\frac{\alpha s}{2}) & \cos(\frac{\alpha s}{2}) & 0\\ 0 & 0 & \cos(\frac{\alpha s}{2})\\ 0 & 0 & -\sin(\frac{\alpha s}{2}) \end{bmatrix},$$

which gives a second-variation operator $\mathcal{S} = \mathcal{S}_1 + \lambda\mathcal{S}_2$ with

$$\begin{aligned}
\mathcal{S}_1\boldsymbol{\zeta} \equiv &\begin{bmatrix} -4K_1 & 0 & 0\\ 0 & -4K_2 & 0\\ 0 & 0 & -4K_3 \end{bmatrix}\boldsymbol{\zeta}'' + \begin{bmatrix} 0 & 4\alpha(K_1+K_2-K_3) & 0\\ -4\alpha(K_1+K_2-K_3) & 0 & 0\\ 0 & 0 & 0 \end{bmatrix}\boldsymbol{\zeta}'\\
&+ \begin{bmatrix} 4\alpha^2(K_2-K_3) & 0 & 0\\ 0 & 4\alpha^2(K_1-K_3) & 0\\ 0 & 0 & 0 \end{bmatrix}\boldsymbol{\zeta}
\end{aligned} \tag{6.1}$$

and

$$\mathcal{S}_2\boldsymbol{\zeta} \equiv \begin{bmatrix} -4 & 0 & 0 \\ 0 & -4 & 0 \\ 0 & 0 & 0 \end{bmatrix} \boldsymbol{\zeta}. \tag{6.2}$$

For this choice of $\mathbf{\Pi}$, the projected constraints take the explicit form

$$\mathbf{T}_1(s) = \begin{bmatrix} 2\sin(\alpha s) \\ 2\cos(\alpha s) \\ 0 \end{bmatrix}, \quad \mathbf{T}_2(s) = \begin{bmatrix} -2\cos(\alpha s) \\ 2\sin(\alpha s) \\ 0 \end{bmatrix}.$$

6.1.1. Verification of hypotheses from section 4. Before applying the results of section 4, we remove the third component of $\boldsymbol{\zeta}$, which plays a trivial role. Any variation $\boldsymbol{\zeta}$ can be written as $\boldsymbol{\zeta} = \bar{\boldsymbol{\zeta}} + \boldsymbol{\zeta}^*$, where $\bar{\boldsymbol{\zeta}}$ contains zeros in the first two slots, and $\boldsymbol{\zeta}^*$ contains a zero in the third slot. Using the explicit form for $\mathcal{S}$, and integrating by parts,

$$\langle \bar{\boldsymbol{\zeta}}, \mathcal{S}\bar{\boldsymbol{\zeta}} \rangle = 4K_3 \langle \bar{\boldsymbol{\zeta}}', \bar{\boldsymbol{\zeta}}' \rangle \geq 0. \tag{6.3}$$

By (6.1) and (6.2), $\mathcal{S}\bar{\boldsymbol{\zeta}}$ contains zeros in the first two slots, and $\mathcal{S}\boldsymbol{\zeta}^*$ contains a zero in the third slot, and, therefore,

$$\langle \boldsymbol{\zeta}, \mathcal{S}\boldsymbol{\zeta} \rangle = \langle \bar{\boldsymbol{\zeta}} + \boldsymbol{\zeta}^*, \mathcal{S}(\bar{\boldsymbol{\zeta}} + \boldsymbol{\zeta}^*) \rangle = \langle \bar{\boldsymbol{\zeta}}, \mathcal{S}\bar{\boldsymbol{\zeta}} \rangle + \langle \boldsymbol{\zeta}^*, \mathcal{S}\boldsymbol{\zeta}^* \rangle \geq \langle \boldsymbol{\zeta}^*, \mathcal{S}\boldsymbol{\zeta}^* \rangle. \tag{6.4}$$

So, given any basis $\boldsymbol{\zeta}_1, \ldots, \boldsymbol{\zeta}_n$ for a maximal subspace on which $\langle \boldsymbol{\zeta}, \mathcal{S}\boldsymbol{\zeta} \rangle < 0$, the vectors $\boldsymbol{\zeta}_1^*, \ldots, \boldsymbol{\zeta}_n^*$ must be linearly independent as functions of s since otherwise some linear combination of $\boldsymbol{\zeta}_1, \ldots, \boldsymbol{\zeta}_n$ would have zeros in the first two slots and hence a nonnegative second variation by (6.3). Then, by (6.4), the span of $\boldsymbol{\zeta}_1^*, \ldots, \boldsymbol{\zeta}_n^*$ is also an n-dimensional (hence maximal) subspace on which $\langle \boldsymbol{\zeta}, \mathcal{S}\boldsymbol{\zeta} \rangle < 0$. Thus we may restrict our attention to variations $\boldsymbol{\zeta}$ with a zero in the third slot.

Thus we define

$$\boldsymbol{\zeta}^* = \begin{bmatrix} \zeta_1 \\ \zeta_2 \end{bmatrix}, \quad \mathbf{T}_1^* = \begin{bmatrix} 2\sin(\alpha s) \\ 2\cos(\alpha s) \end{bmatrix}, \quad \mathbf{T}_2^* = \begin{bmatrix} -2\cos(\alpha s) \\ 2\sin(\alpha s) \end{bmatrix},$$

and

$$\mathcal{H}_d^{cons,*} = \{\boldsymbol{\zeta}^* \in H^2(\mathbb{R}^2, (0,1)) : \boldsymbol{\zeta}^*(0) = \boldsymbol{\zeta}^*(1) = \mathbf{0}, \ \langle \boldsymbol{\zeta}^*, \mathbf{T}_1^* \rangle = \langle \boldsymbol{\zeta}^*, \mathbf{T}_2^* \rangle = 0\}.$$

Plugging $\boldsymbol{\zeta}^*$ into (4.1), we find

$$(\mathcal{S}_3 + \lambda \mathcal{S}_4)\boldsymbol{\zeta}^* = \breve{c}_1 \mathbf{T}_1^* + \breve{c}_2 \mathbf{T}_2^*, \quad \boldsymbol{\zeta}^* \in \mathcal{H}_d^{cons,*}, \tag{6.5}$$

where

$$\begin{aligned} \mathcal{S}_3\boldsymbol{\zeta}^* \equiv \begin{bmatrix} -4K_1 & 0 \\ 0 & -4K_2 \end{bmatrix} (\boldsymbol{\zeta}^*)'' &+ \begin{bmatrix} 0 & 4\alpha(K_1 + K_2 - K_3) \\ -4\alpha(K_1 + K_2 - K_3) & 0 \end{bmatrix} (\boldsymbol{\zeta}^*)' \\ &+ \begin{bmatrix} 4\alpha^2(K_2 - K_3) & 0 \\ 0 & 4\alpha^2(K_1 - K_3) \end{bmatrix} \boldsymbol{\zeta}^*, \\ \mathcal{S}_4\boldsymbol{\zeta}^* \equiv \begin{bmatrix} -4 & 0 \\ 0 & -4 \end{bmatrix} \boldsymbol{\zeta}^*. \end{aligned}$$

If we let $\mathcal{Q}$ denote the projection onto the space of functions L^2-orthogonal to both $\mathbf{T}_1^*$ and $\mathbf{T}_2^*$, then (6.5) may be rewritten as $(\mathcal{Q}\mathcal{S}_3\mathcal{Q})\boldsymbol{\zeta}^* = 4\lambda\boldsymbol{\zeta}^*$ for $\boldsymbol{\zeta}^* \in \mathcal{H}_d^{cons,*}$. We thus have an eigenvalue problem for the operator $\mathcal{Q}\mathcal{S}_3\mathcal{Q}$ on the space $\mathcal{H}_d^{cons,*}$. Relying on the fact that the spectrum of $\mathcal{S}$ in $\mathcal{H}_d$ consists purely of isolated eigenvalues, each with finite multiplicity, one can show that $\mathcal{S}_3$ has the same type of spectrum (see the argument on p. 3067 of [19]). It then follows from the spectral theorem for self-adjoint operators [8, p. 233] that the solutions of this equation form an orthogonal basis for $\mathcal{H}_d^{cons,*}$. Using the eigenvalue equation, we can see that this basis is also $(\mathcal{S}_3 + \lambda\mathcal{S}_4)$-orthogonal, as we need to apply Lemma 3.1.

6.1.2. Determination of the index. We observe that, for any continuous $\boldsymbol{\zeta}^* = (\zeta_1, \zeta_2)$ with ζ_1 and ζ_2 not both identically zero,

$$\langle \boldsymbol{\zeta}^*, \mathcal{S}_4\boldsymbol{\zeta}^* \rangle = -4\int_0^1 (\zeta_1(s)^2 + \zeta_2(s)^2)ds < 0.$$

Therefore, by Lemma 4.1, the index of the unbuckled equilibrium at (α, λ) is equal to the number of branch points λ_n below λ at that particular angle α. Thus, once we have determined the branch points, we will have determined the index at any (α, λ).

The differential equation appearing in (6.5) can be written out explicitly (after dividing through by $-4K_1$) as

$$\begin{aligned}
\zeta_1'' - A\zeta_2' + B\zeta_1 &= -\frac{\sin(\alpha s)\check{c}_1}{2K_1} + \frac{\cos(\alpha s)\check{c}_2}{2K_1}, \\
\rho\zeta_2'' + A\zeta_1' + C\zeta_2 &= -\frac{\cos(\alpha s)\check{c}_1}{2K_1} - \frac{\sin(\alpha s)\check{c}_2}{2K_1},
\end{aligned}$$

where $\gamma = K_3/K_1$, $\rho = K_2/K_1$, $A = \alpha(1+\rho-\gamma)$, $B = \alpha^2(\gamma-\rho)+\frac{\lambda}{K_1}$, and $C = \alpha^2(\gamma-1)+\frac{\lambda}{K_1}$. The general solution can be found in closed form, and, applying the four boundary conditions $\zeta_{1,2}(0) = \zeta_{1,2}(1) = 0$ and two linearized constraints, we see that branch points occur when

$$\det \begin{bmatrix} \mathbf{M}_1(0) & \mathbf{M}_2(0) & \mathbf{M}_3(0) \\ \mathbf{M}_1(1) & \mathbf{M}_2(1) & \mathbf{M}_3(1) \\ \int_0^1 \mathbf{T}(s)^T\mathbf{M}_1(s)ds & \int_0^1 \mathbf{T}(s)^T\mathbf{M}_2(s)ds & \int_0^1 \mathbf{T}(s)^T\mathbf{M}_3(s)ds \end{bmatrix} = 0, \tag{6.6}$$

where $\mathbf{T}(s) \equiv \begin{bmatrix} \mathbf{T}_1^*(s) & \mathbf{T}_2^*(s) \end{bmatrix}$,

$$\mathbf{M}_{1,2}(s) = \begin{bmatrix} \sigma_{1,2}\cos(\sqrt{\omega_{1,2}}s) & -\sigma_{1,2}\sin(\sqrt{\omega_{1,2}}s) \\ \sin(\sqrt{\omega_{1,2}}s) & \cos(\sqrt{\omega_{1,2}}s) \end{bmatrix}, \quad \mathbf{M}_3(s) = -\frac{1}{2\lambda}\begin{bmatrix} \sin(\alpha s) & -\cos(\alpha s) \\ \cos(\alpha s) & \sin(\alpha s) \end{bmatrix}$$

for ω_1, ω_2, the (possibly complex) quantities

$$\omega_{1,2} = \frac{A^2 + B\rho + C \pm \sqrt{(A^2 + B\rho + C)^2 - 4BC\rho}}{2\rho},$$

and

$$\sigma_{1,2} = -\frac{A\sqrt{\omega_{1,2}}}{\omega_{1,2} - B}.$$

(We note that, for a few isolated parameter values, the characteristic equation of (6.5) has repeated roots, so the branch point equation does not take the above form.)

Further simplification of the determinant of this 6-by-6 matrix is difficult, so we instead determine its zeros numerically in the results in section 6.3 (taking care to handle separately the special cases where the characteristic equation has repeated roots). However, in the case when $K_1 = K_2$, this numerical search for zeros is difficult to implement since, due to symmetry, the above determinant does not cross zero transversely but rather intersects it tangentially. Thus we present in the next section a separate derivation of the index for an isotropic strut $K_1 = K_2$.

6.2. The isotropic strut. When $K_1 = K_2$, we choose a slightly different projection matrix:

$$\mathbf{\Pi}(s) \equiv \begin{bmatrix} \cos(\frac{\alpha s}{2}) & \sin(\frac{\alpha s}{2}) & 0 \\ -\sin(\frac{\alpha s}{2}) & \cos(\frac{\alpha s}{2}) & 0 \\ 0 & 0 & \cos(\frac{\alpha s}{2}) \\ 0 & 0 & -\sin(\frac{\alpha s}{2}) \end{bmatrix}.$$

Then the second-variation operator is $\mathcal{S} = \mathcal{S}_1 + \lambda \mathcal{S}_2$, where

$$\mathcal{S}_1 \boldsymbol{\zeta} \equiv \begin{bmatrix} -4K_1 & 0 & 0 \\ 0 & -4K_1 & 0 \\ 0 & 0 & -4K_3 \end{bmatrix} \boldsymbol{\zeta}'' + \begin{bmatrix} 0 & -4\alpha K_3 & 0 \\ 4\alpha K_3 & 0 & 0 \\ 0 & 0 & 0 \end{bmatrix} \boldsymbol{\zeta}'$$

and

$$\mathcal{S}_2 \boldsymbol{\zeta} \equiv \begin{bmatrix} -4 & 0 & 0 \\ 0 & -4 & 0 \\ 0 & 0 & 0 \end{bmatrix} \boldsymbol{\zeta}.$$

The projected constraints take the explicit form

$$\mathbf{T}_1(s) = \begin{bmatrix} 0 \\ 2 \\ 0 \end{bmatrix}, \quad \mathbf{T}_2(s) = \begin{bmatrix} -2 \\ 0 \\ 0 \end{bmatrix}.$$

We may follow the same procedure as in section 6.1.1 to show that the set of solutions to (6.5) forms a basis for $\mathcal{H}_d^{cons,*}$, with the operator $\mathcal{S}_3$ now taking the form

$$\mathcal{S}_3 \boldsymbol{\zeta}^* \equiv \begin{bmatrix} -4K_1 & 0 \\ 0 & -4K_1 \end{bmatrix} (\boldsymbol{\zeta}^*)'' + \begin{bmatrix} 0 & -4\alpha K_3 \\ 4\alpha K_3 & 0 \end{bmatrix} (\boldsymbol{\zeta}^*)'.$$

For any continuous $\boldsymbol{\zeta}^* = (\zeta_1, \zeta_2)$ with ζ_1 and ζ_2 not both identically zero,

$$\langle \boldsymbol{\zeta}^*, \mathcal{S}_4 \boldsymbol{\zeta}^* \rangle = -4 \int_0^1 (\zeta_1(s)^2 + \zeta_2(s)^2) ds < 0,$$

and thus, by the theory of section 4, the index of the unbuckled equilibrium at (α, λ) is equal to the number of branch points λ_n below λ at that particular angle α.

The differential equation appearing in (6.5) can be written out explicitly (after dividing through by $-4K_1$) as

$$\zeta_1'' + A\zeta_2' + B\zeta_1 = \frac{\breve{c}_2}{2K_1},$$
$$\zeta_2'' - A\zeta_1' + B\zeta_2 = -\frac{\breve{c}_1}{2K_1},$$

where $\gamma = K_3/K_1$, $A = \gamma\alpha$, and $B = \frac{\lambda}{K_1}$. The general solution can again be found in closed form, and, applying the boundary conditions and constraints, we see that (apart from the special cases $A = 0$, $B = 0$, and $A^2 + 4B = 0$) branch points occur when there is a nontrivial solution $(C_1, C_2, C_3, C_4, \breve{c}_1, \breve{c}_2)$ to

$$\begin{bmatrix} 1 & 0 & 1 & 0 & 0 & \frac{1}{2K_1B} \\ 0 & -1 & 0 & -1 & -\frac{1}{2K_1B} & 0 \\ \cos\omega_1 & \sin\omega_1 & \cos\omega_2 & \sin\omega_2 & 0 & \frac{1}{2K_1B} \\ \sin\omega_1 & -\cos\omega_1 & \sin\omega_2 & -\cos\omega_2 & -\frac{1}{2K_1B} & 0 \\ \frac{2(1-\cos\omega_1)}{\omega_1} & -\frac{2\sin\omega_1}{\omega_1} & \frac{2(1-\cos\omega_2)}{\omega_2} & -\frac{2\sin\omega_2}{\omega_2} & -\frac{1}{K_1B} & 0 \\ -\frac{2\sin\omega_1}{\omega_1} & -\frac{2(1-\cos\omega_1)}{\omega_1} & -\frac{2\sin\omega_2}{\omega_2} & -\frac{2(1-\cos\omega_2)}{\omega_2} & 0 & -\frac{1}{K_1B} \end{bmatrix} \begin{bmatrix} C_1 \\ C_2 \\ C_3 \\ C_4 \\ \breve{c}_1 \\ \breve{c}_2 \end{bmatrix} = \begin{bmatrix} 0 \\ 0 \\ 0 \\ 0 \\ 0 \\ 0 \end{bmatrix},$$

where $\omega_{1,2}$ are the (possibly complex) quantities $\frac{A \pm \sqrt{A^2+4B}}{2}$.

Denote the upper-left 4-by-4 block of this 6-by-6 matrix as $\mathbf{M}_{11}$, the upper-right 4-by-2 block as $\mathbf{M}_{12}$, the lower-left 2-by-4 block as $\mathbf{M}_{21}$, and the lower-right 2-by-2 block as $\mathbf{M}_{22}$. Then $\det \mathbf{M}_{11} = 2(1 - \cos(\omega_1 - \omega_2))$. As long as $\omega_1 - \omega_2 \neq 2n\pi$, $n = 1, 2, 3, \ldots$, we then find that

$$\begin{bmatrix} C_1 \\ C_2 \\ C_3 \\ C_4 \end{bmatrix} = -\mathbf{M}_{11}^{-1}\mathbf{M}_{12} \begin{bmatrix} \breve{c}_1 \\ \breve{c}_2 \end{bmatrix}. \tag{6.7}$$

Thus

$$-\mathbf{M}_{21}\mathbf{M}_{11}^{-1}\mathbf{M}_{12} \begin{bmatrix} \breve{c}_1 \\ \breve{c}_2 \end{bmatrix} + \mathbf{M}_{22} \begin{bmatrix} \breve{c}_1 \\ \breve{c}_2 \end{bmatrix} = \begin{bmatrix} 0 \\ 0 \end{bmatrix}.$$

Simplifying the above equation, we find

$$\frac{1}{K_1 B\omega_1\omega_2 \sin\left(\frac{\omega_1-\omega_2}{2}\right)} \left(2(\omega_1 - \omega_2)\sin\frac{\omega_1}{2}\sin\frac{\omega_2}{2} - \omega_1\omega_2 \sin\left(\frac{\omega_1 - \omega_2}{2}\right)\right) \begin{bmatrix} 1 & 0 \\ 0 & 1 \end{bmatrix} \begin{bmatrix} \breve{c}_1 \\ \breve{c}_2 \end{bmatrix} = \begin{bmatrix} 0 \\ 0 \end{bmatrix}. \tag{6.8}$$

Thus, we have only the trivial solution $\breve{c}_1 = \breve{c}_2 = C_1 = C_2 = C_3 = C_4 = 0$ unless

$$2(\omega_1 - \omega_2)\sin\frac{\omega_1}{2}\sin\frac{\omega_2}{2} - \omega_1\omega_2 \sin\left(\frac{\omega_1 - \omega_2}{2}\right) = 0,$$

or, in terms of A and B:

$$2\sqrt{A^2+4B}\sin\frac{A+\sqrt{A^2+4B}}{4}\sin\frac{A-\sqrt{A^2+4B}}{4}+B\sin\left(\frac{\sqrt{A^2+4B}}{2}\right)=0. \tag{6.9}$$

If this condition does hold, then any $(\check{c}_1,\check{c}_2)$ will satisfy (6.8), with (C_1,C_2,C_3,C_4) then determined by (6.7). Thus we have a branch point when (6.9) holds, and the corresponding conjugate point has multiplicity two.

A check of the special cases $\omega_1-\omega_2=2n\pi$, $n=1,2,3,\ldots$, reveals that the conjugate point condition again takes the form (6.9), again with each conjugate point having multiplicity two.

In the special cases $A=0$, $B=0$, and $A^2+4B=0$, the general solution used above is not valid, but we may directly analyze these cases to find the following:

- The case $B=0, A\neq 0$ yields the branch point condition

$$\frac{A}{2}\cos\left(\frac{A}{2}\right)=\sin\left(\frac{A}{2}\right), \tag{6.10}$$

  which matches the dominant term in a Taylor series expansion of (6.9) in the limit that $B\to 0$. Again, the conjugate points in this case have multiplicity 2.
- The case $A=0, B\neq 0$ yields the branch condition

$$\sqrt{B}\sin(\sqrt{B})-4\sin^2\left(\frac{\sqrt{B}}{2}\right)=0,$$

  which matches (6.9) when $A=0$. Again, the conjugate points in this case have multiplicity 2.
- The case $A^2+4B=0$ can exhibit no branch points.

In summary, branch points are the solutions to (6.9) when $B\neq 0$ and $A^2+4B\neq 0$. When $A^2+4B=0$, there are no branch points, while, when $B=0$, they are the solutions to (6.10).

6.3. Results. In Figure 6.1, we show the index of the unbuckled configuration (color-coded by the scheme given in Figure 6.2) for various values of the twist angle α, loading force λ, bending stiffness ratio ρ, and twisting-to-bending stiffness ratio γ. In each frame of the figure, the black lines indicate the locations of the branch points as a function of α and λ/K_1 for ρ and γ held fixed. The top row of frames is for the isotropic problem $\rho=1$, so the lines were determined by (6.9), while, for the remaining frames, they were determined using (6.6). The coloring of the diagrams is a computation of the index via the numerical conjugate point test described in section 2 and verifies the result proven in this section, namely, that the index at a point $(\alpha,\lambda/K_1)$ is equal to the number of lines that lie below it. (In the isotropic case $\rho=1$, each line is counted with multiplicity two, as shown in section 6.2.)

The stability results in the isotropic case $\rho=1$ match the standard intuition about buckling. For zero twist, the unbuckled configuration is stable up to a maximal loading force and becomes more and more unstable thereafter. As twist (either negative or positive) is added, the same behavior is observed, except that the threshold for instability is lowered since the twist destabilizes the unbuckled configuration.

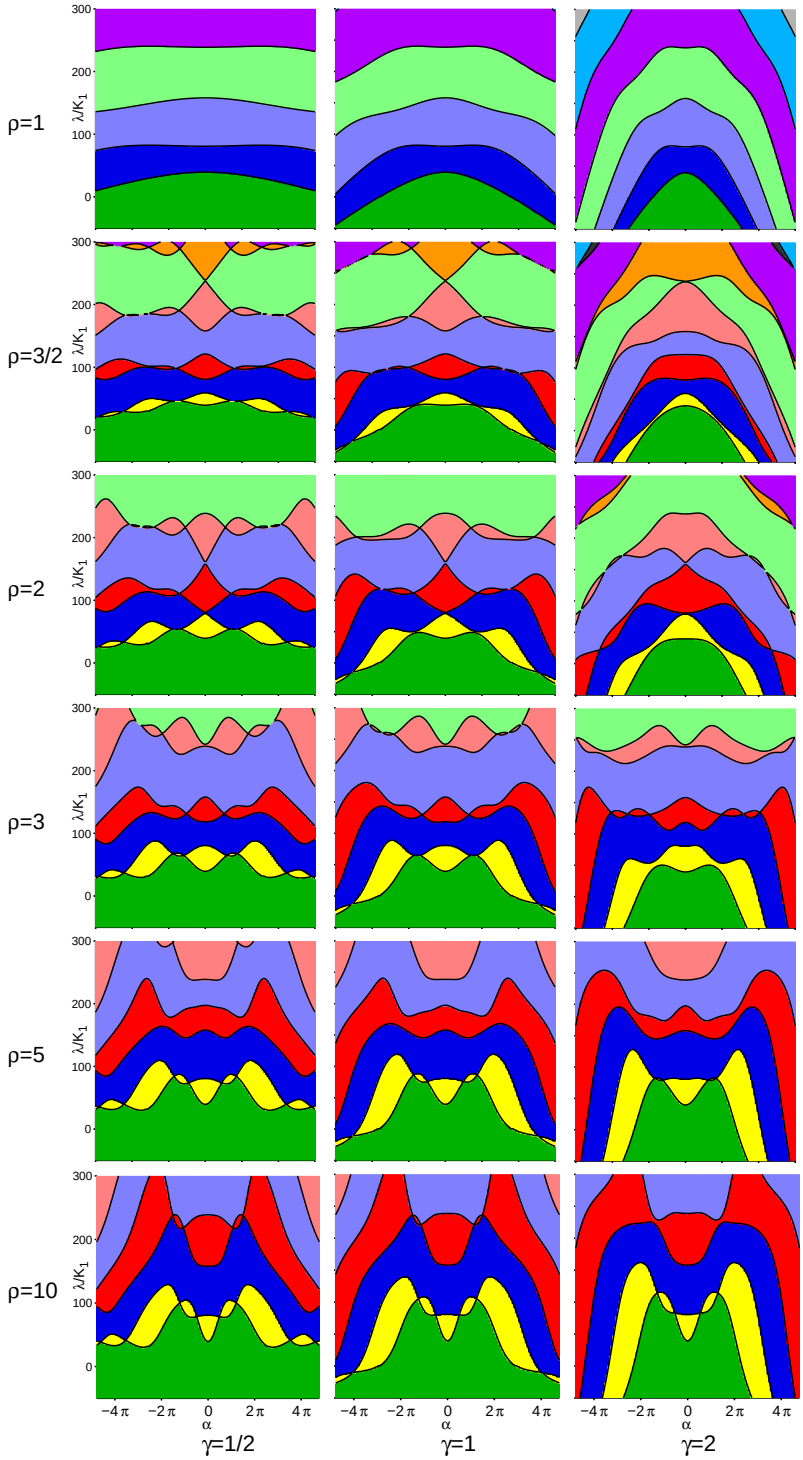

Figure 6.1. *The index on the plane of unbuckled equilibria for various values of ρ, the ratio of bending stiffnesses, and of γ, the ratio of twisting to bending stiffness. In each graph, the index of the unbuckled equilibrium with twist angle α and endloading λ is indicated by color, following the scheme in Figure 6.2. Black curves indicate the set of branch points as determined by the analysis in sections 6.1 and 6.2.*

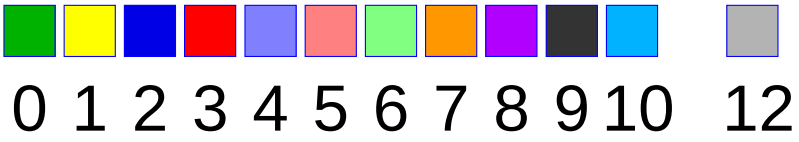

Figure 6.2. *Color scheme used to represent the index (index* 11 *is omitted since it does not appear in any of our figures).*

Comparing the $\rho = 1$ row to the $\rho = 3/2$ row, we can see the splitting generated by the anisotropy, as each curve where the index jumps by two when $\rho = 1$ splits into a pair of interlaced curves, where the index jumps by one when $\rho = 3/2$. As ρ grows, we also note a prominent trend whereby a twist angle α can cause a stabilization of the first buckling mode, as seen by the emergence of two protuberances symmetrically about $\alpha = 0$, e.g., at $\rho = 3/2$ for $\gamma = 1/2$, at $\rho = 2$ for $\gamma = 1$, or at $\rho = 3$ for $\gamma = 2$. Physically, this corresponds to the fact that an imposed twist effectively transfers some of the enhanced bending stiffness K_2 to the direction governed by K_1 in the untwisted configuration. For α sufficiently large, this effect is eventually countered by the fact that the act of twisting itself imposes a certain degree of instability so that the green-yellow boundary curve eventually begins to decrease for values of α further from the line $\alpha = 0$. As ρ increases further, the protuberances become larger. The bands with higher index mimic the shape of the green (stable) region.

As γ decreases, we can see that the dominant trend is simply to stretch the diagram laterally away from $\alpha = 0$. In the isotropic case, this stretching transformation is obeyed exactly. (We can see in the theoretical derivation that the index depends on α only through the term $\alpha\gamma$.) In the anisotropic case, a change in γ causes some slight qualitative changes in the index diagram in addition to this lateral stretch.

We note that we have restricted ρ to be greater than 1 in Figure 6.1 since any $\rho < 1$ diagram may be deduced from an appropriate $\rho > 1$ diagram. Specifically, given $\rho < 1$ and any values for γ and K_1, we have a strut with weaker bending stiffness equal to K_2, stronger bending stiffness equal to $1/\rho$ times the weaker bending stiffness ($K_1 = (1/\rho)K_2$), and twisting stiffness equal to γ/ρ times the weaker bending stiffness ($K_3 = (\gamma/\rho)K_2 = \gamma K_1$). Thus, if we consider the diagram with $\rho^* = 1/\rho > 1$ and $\gamma^* = \gamma/\rho$ and relabel the y-axis as λ/K_2 rather than λ/K_1, we will have the correct index diagram for (K_1, K_2, K_3). (If one wants a diagram with λ/K_1 to match the other diagrams, one would simply scale vertically by $K_1/K_2 = 1/\rho$.)

7. Stability of buckled configurations.

7.1. "Slices" of the sheets of buckled equilibria.

In the previous section, for fixed values of ρ and γ, the index of each unbuckled configuration in the $\alpha - \lambda$ plane was determined. The curves on this plane where the index changes indicate where sheets of buckled equilibria intersect this plane. In this section, we discuss these sheets of buckled equilibria. They are fairly complicated due to folding and branching, so we compute only those portions of the sheets corresponding to some of the simplest buckled configurations.

To build up to displaying the sheets of buckled equilibria, we first consider "slices" in which the angle α is fixed, while the force λ is allowed to vary. For example, we consider $(\rho, \gamma) = (1, 1)$

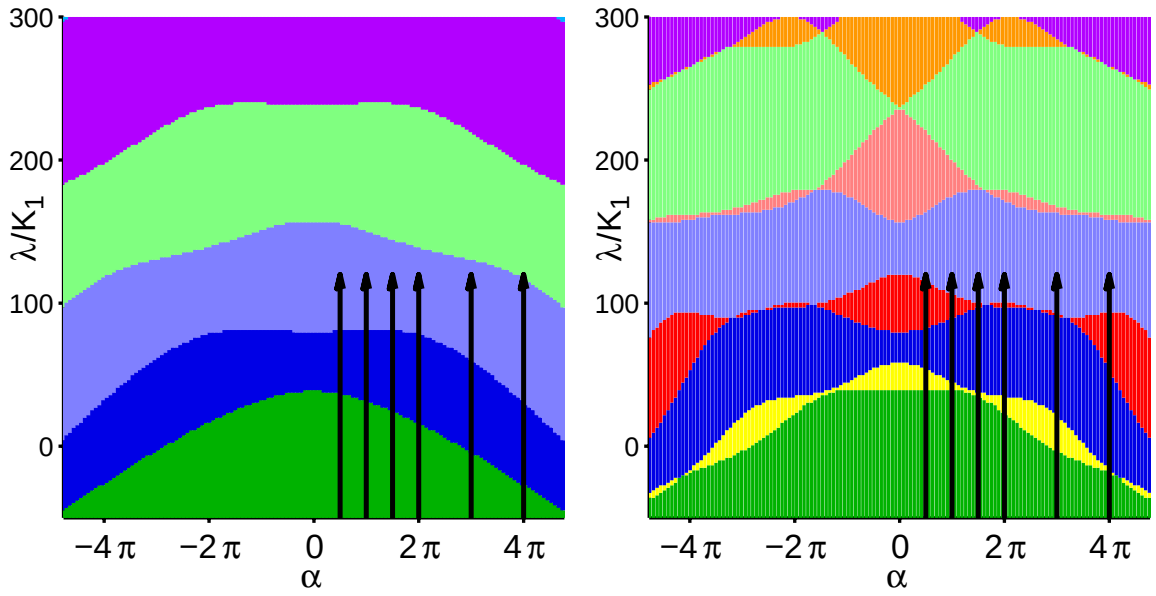

Figure 7.1. *A buckling problem at various values of the twist angle α. For bending stiffness ratios $\rho = 1$ (left) and $\rho = 3/2$ (right) and twisting-to-bending stiffness ratio $\gamma = 1$, we show the plane of unbuckled equilibria colored by stability from Figure 6.1. Now we fix α at several values ($\pi/2$, π, $3\pi/2$, 2π, 3π, and 4π) and vary the force λ. Branches of buckled configurations will bifurcate at each point where an arrow meets a change in color.*

and $(\frac{3}{2}, 1)$. In each case, we fix several values of α, namely, $\alpha = \frac{\pi}{2}, \pi, \frac{3\pi}{2}, 2\pi, 3\pi, 4\pi$, and then we vary the force λ, as shown in Figure 7.1.

For each slice, we compute one-dimensional branches of buckled equilibria using AUTO [5, 6], which uses numerical parameter continuation to compute solutions to boundary value problems (BVPs) such as we have here with the Euler–Lagrange equations in $\mathbf{q}(s)$ subject to the constraints in (5.1). We present here only the briefest of introductions to continuation methods and refer the reader to [5, 6] and references therein for a full description.

As the name suggests, numerical parameter continuation is the computation of a family of solutions to a BVP as a parameter (in this case, λ) is varied. After discretization in s, the BVP becomes a finite-dimensional equation of the form

$$\mathbf{F}(\mathbf{X}) = \mathbf{0}, \qquad \mathbf{F} : \mathbb{R}^{n+1} \to \mathbb{R}^n. \tag{7.1}$$

This system has one more variable than it has equations; the extra variable is the continuation parameter λ. Therefore, given a solution $\mathbf{X}_0$, there generally exists a locally unique one-dimensional family of points, called a solution branch, that passes through $\mathbf{X}_0$. AUTO computes a numerical approximation to this solution branch using a well-known algorithm called the *pseudoarclength continuation method* [15]. As implemented in AUTO, branch points where new solution branches intersect the current branch can be detected and followed, and thus we may begin with a known solution $\mathbf{X}_0$ on the plane of unbuckled equilibria, follow solutions numerically on this plane, and then detect and follow the bifurcating branches which emerge at the color changes in Figure 7.1.

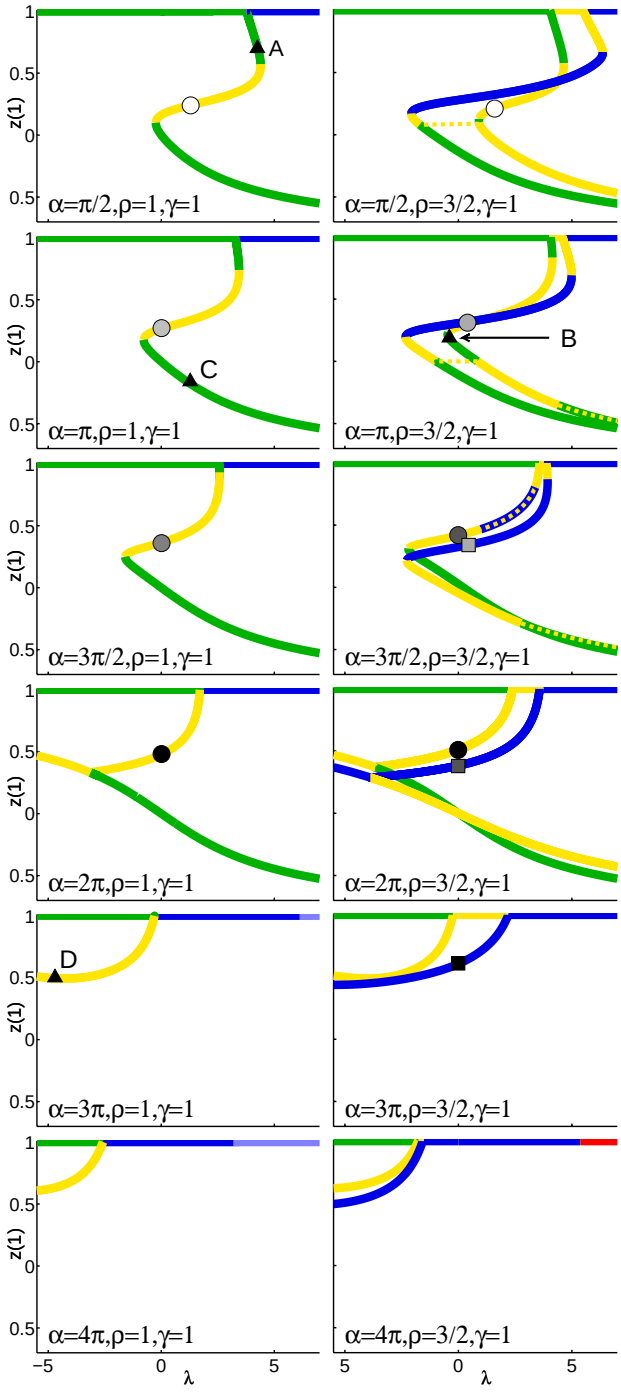

Figure 7.2. *Force-length diagrams for several values of the twist angle α and the bending stiffness ratio ρ: $\rho = 1$ in the left column, and $\rho = 3/2$ in the right column; α increases from $\pi/2$ to 4π vertically; $\gamma = 1, K_1 = 0.1$ throughout. In each graph, the length $z(1)$ is plotted against the force λ. Branches are colored by stability index, using the color scheme from Figure 6.2. Horizontal branches represent unbuckled configurations. For $\rho = 1$, we show the branch of buckled configurations arising from the first branch point, which splits into the two branches shown in the $\rho = 3/2$ diagrams. Some secondary bifurcating branches are shown as dashed lines. Circles and squares indicate points at the edges of the surfaces in Figures 7.9 and 7.11. Triangles with corresponding letters* A–D *indicate configurations depicted in Figure 7.3.*

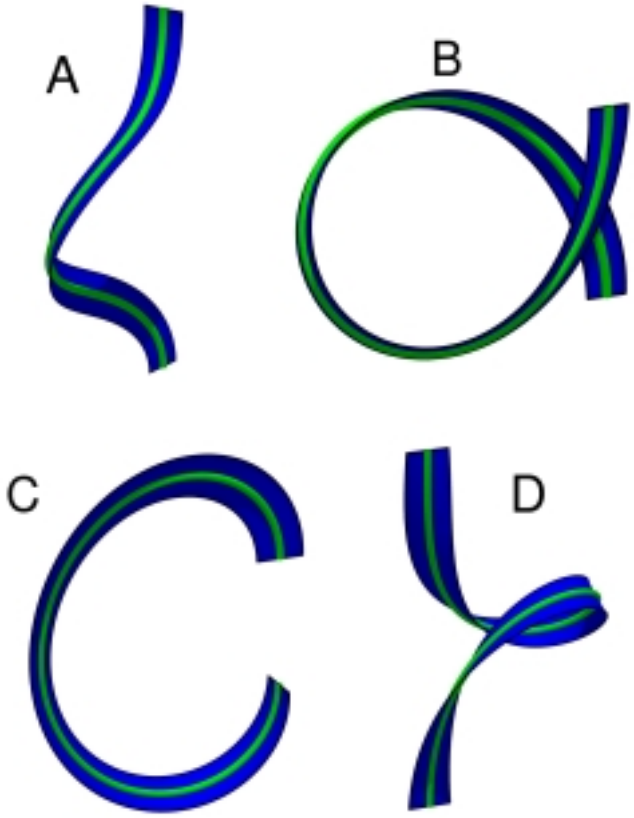

Figure 7.3. *Physical configurations appearing in the bifurcation diagrams in Figure 7.2. The centerline of the strut is shown as a green tube, while the director* $\mathbf{d}_1$ *is shown as a blue ribbon.*

To visualize these branches, we create force-length bifurcation diagrams, i.e., two-dimensional graphs that plot the force λ against the "length" $z(1)$, the distance between the two ends of the strut. (Thus negative lengths indicate that the endpoint of the strut corresponding to $s = 1$ has passed through the origin to the other side of the z-axis.) Figure 7.2 contains diagrams for the simplest buckling solutions. For the isotropic problem $\rho = 1$, these simple solutions arise from the first branch point, the green-to-blue transition on the plane of unbuckled equilibria. In the anisotropic problem $\rho = \frac{3}{2}$, these simple solutions perturb to two branches of solutions, the green-to-yellow and the yellow-to-blue transitions on the plane of unbuckled equilibria.

Some sample physical configurations appearing in these bifurcation diagrams are shown in Figure 7.3. Configurations close to the plane of unbuckled equilibria contain a small amount of buckling, as in configuration A, reminiscent of the first buckling mode of the classic untwisted problem. For some values of α, these are initially stable and then become unstable at a fold in λ, while, for sufficiently high α, they are always unstable. Further down the branch are more drastically buckled configurations, still with positive length, such as configuration B. Some of these are stable, as seen in the portions of the lowermost green branches that have $z(1) > 0$. There are also negative length configurations such as configuration C, and, again, some of

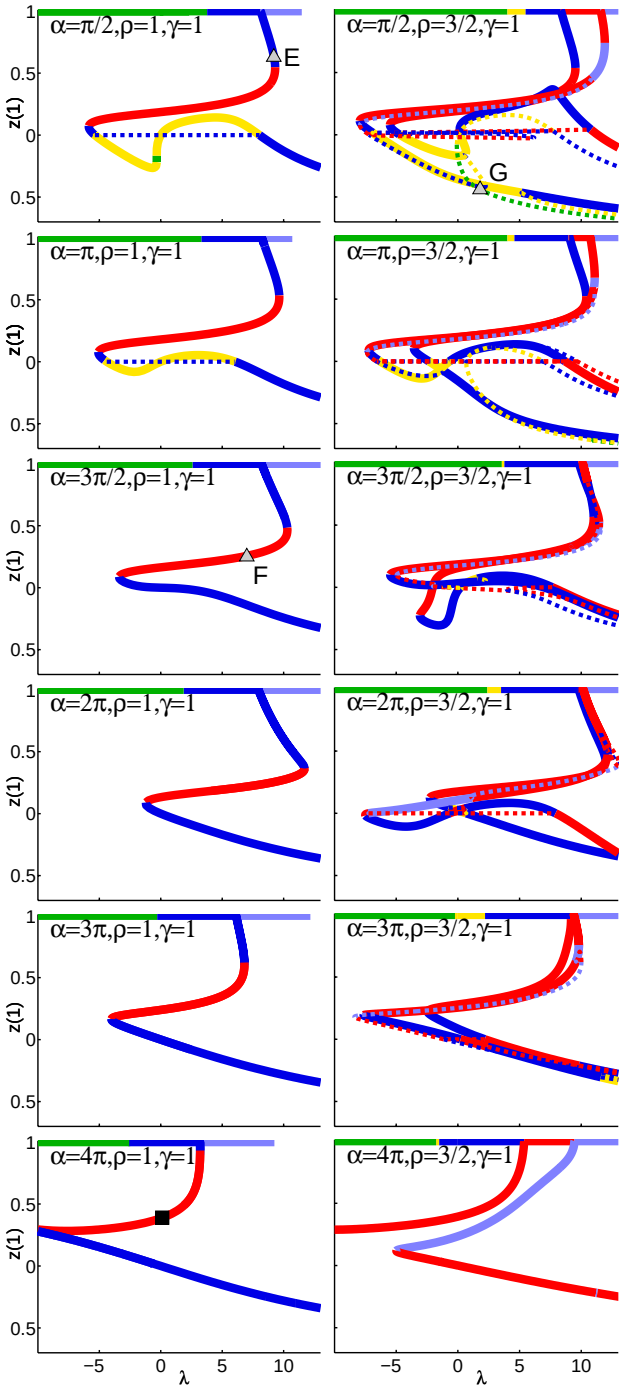

Figure 7.4. *Force-length diagrams for the next-higher buckling modes as compared to those shown in Figure 7.2. For $\rho = 1$, $\gamma = 1$, we plot the branch of buckled configurations arising from the second branch point, while, for $\rho = 3/2$, $\gamma = 1$, we plot the branches of buckled configurations arising from the third and fourth branch points, which are the splitting of the branch in the first column. The square in the lower left graph indicates a point at the edge of the surface in Figure 7.9. Triangles with corresponding letters* E–G *indicate configurations depicted in Figure 7.5.*

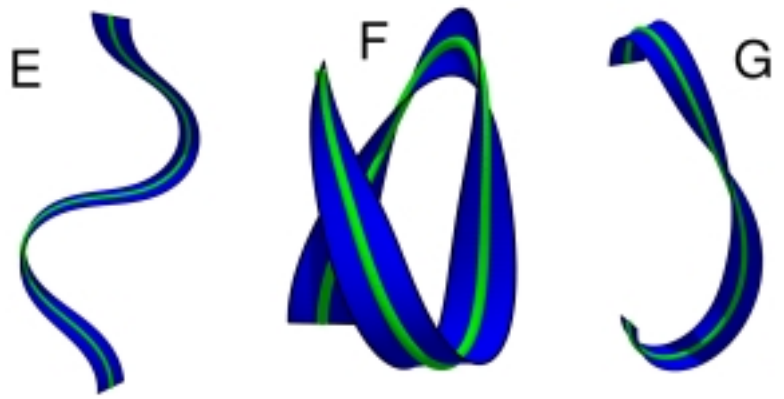

Figure 7.5. *Physical configurations appearing in the bifurcation diagrams in Figure 7.4. The centerline of the strut is shown as a green tube, while the director* $\mathbf{d}_1$ *is shown as a blue ribbon.*

these are stable. Finally, in some diagrams, there are branches leaving the graph at the left edge; the corresponding configurations look like configuration D, and are all unstable. The anisotropic diagrams are relatively simple splittings of the isotropic diagrams into two images, although there are a few secondary bifurcating branches that appear, sometimes connecting the two images to each other, and in one case ($\alpha = \frac{3\pi}{2}, \rho = \frac{3}{2}$) connecting a branch to itself.

Figure 7.4 illustrates the next-simplest buckling configurations. For the isotropic problem, these solutions arise from the second branch point, the blue-to-light-blue transition on the plane of unbuckled equilibria; for the anisotropic problem, these solutions perturb to two branches of solutions, the blue-to-red and the red-to-light-blue transitions. Some sample physical configurations appearing in these bifurcation diagrams are shown in Figure 7.5. The strut initially buckles to a two-mode shape like configuration E, as in the classic untwisted problem. Further on the branch, there are more drastically buckled configurations such as configuration F. Negative length configurations also exist, such as configuration G; in one case ($\alpha = \frac{\pi}{2}, \rho = \frac{3}{2}$), these are stable. Here, the perturbation in the diagram caused by anisotropy is quite complicated, leading in many cases to multiple secondary bifurcating branches with complicated connectivity. We expect that this complication would only worsen for higher buckling modes.

7.2. The sheets of buckled equilibria. Since AUTO is designed to compute one-dimensional branches of solutions as described in the previous section, it does not directly compute the two-dimensional sheets of buckled equilibria that we are interested in. However, by using a judicious itinerary of parameter switching, one may compute an approximation of the two-dimensional surface using a collection of one-dimensional curves [18, 22].

Consider first the computation of the plane of unbuckled equilibria. Of course, the configurations on this plane are known in closed form, so it is hardly necessary to determine them numerically, but nevertheless it serves as a useful first example. Furthermore, it is computationally expedient to compute this plane numerically since in so doing AUTO will detect branch points to be used as starting points for the computation of the sheets of buckled equilibria. We begin the computation of the plane of unbuckled equilibria at $(\lambda, \alpha) = (0, 0)$. We fix

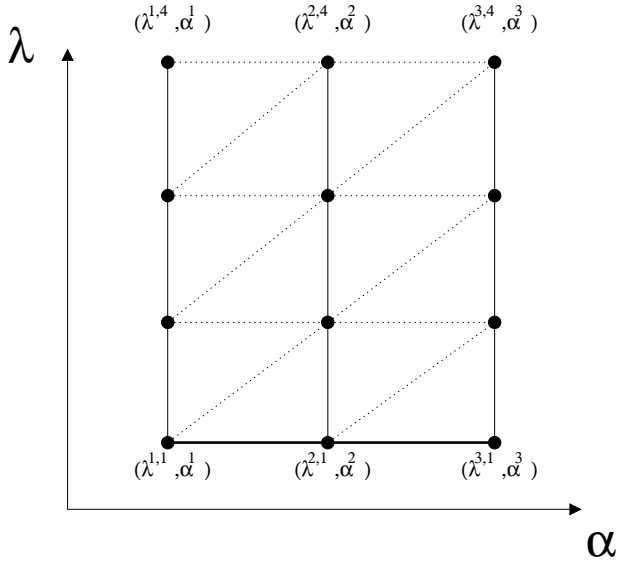

Figure 7.6. *Triangulation of plane of unbuckled equilibria: The solid horizontal line at the bottom of the grid represents the initial calculation fixing λ and allowing α to vary. Each of the solid vertical black lines represents a continuation in λ keeping α fixed. Each $(\lambda^{i,j}, \alpha^i)$ is marked with a black circle, and the triangulation is shown with the dotted lines.*

$\lambda = 0$ and allow α to vary, giving a system of the form (7.1), with α but not λ a component of $\mathbf{X}$. We then perform N steps of the continuation calculation described in section 7.1, giving a solution branch which we will denote by $(\lambda^{i,1}, \alpha^i), 1 \le i \le N$. (Note that $\lambda^{i,1} = 0$ for all i.) We now begin a new one-dimensional continuation calculation at each of the solutions $(\lambda^{i,1}, \alpha^i)$ by fixing $\alpha = \alpha^i$ and allowing λ to vary. This leads to a solution branch which we shall denote by $(\lambda^{i,j}, \alpha^i), 1 \le j \le M$. We choose M to be fixed for all i so that the result is a "grid" of points in the plane of unbuckled equilibria. Even though $\lambda^{i,1} = 0$ for $1 \le i \le N$, it is not necessarily the case that $\lambda^{i,j} = \lambda^{k,j}$ for $j > 1, k \ne i$, since AUTO automatically adapts the step size Δt during the calculation. We then triangulate the plane by choosing as the vertices of our triangles $(\lambda^{i,j}, \alpha^i), (\lambda^{i+1,j}, \alpha^{i+1}), (\lambda^{i+1,j+1}, \alpha^{i+1})$ and $(\lambda^{i,j}, \alpha^i), (\lambda^{i,j+1}, \alpha^i), (\lambda^{i+1,j+1}, \alpha^{i+1})$ for $1 \le i \le N-1, 1 \le j \le M-1$, as shown in Figure 7.6.

The sheets of buckled equilibria are calculated in a similar fashion. During each one-dimensional continuation in λ on the plane of unbuckled equilibria, AUTO is set to automatically report all branch points that it detects. Let $\lambda_k^{i,1}$ denote the value of λ at the kth branch point on the branch with $\alpha = \alpha^i$. We note that, in general, $\lambda_k^{i,1} \ne \lambda_k^{m,1}$ when $m \ne i$ since the position of the branch point is a function of α. At each such branch point, AUTO can be used to switch branches and compute a solution branch on the sheet of buckled equilibria emanating from the branch point. So, similar to the unbuckled case, we have an initial set of solutions $(\lambda_k^{i,1}, \alpha^i)$ from which we perform continuation calculations, keeping α fixed and allowing λ to vary. These calculations give rise to a set of buckled equilibria; we denote the values of λ and α for these equilibria by $(\lambda_k^{i,j}, \alpha^i)$ for $1 \le i \le N$ and $1 \le j \le M$. Finally, we triangulate the kth sheet by choosing the vertices of our triangles to be $(\lambda_k^{i,j}, \alpha^i), (\lambda_k^{i+1,j}, \alpha^{i+1}), (\lambda_k^{i+1,j+1}, \alpha^{i+1})$

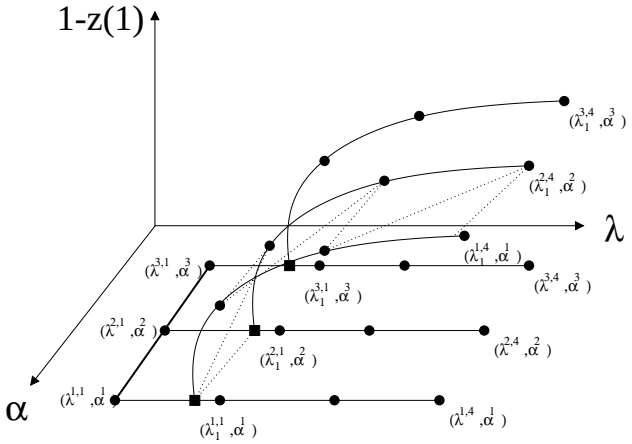

Figure 7.7. *Triangulation of a sheet of buckled equilibria: As in Figure 7.6, the thick black line in the (λ, α) plane represents the initial continuation in α keeping λ fixed, and the thin black lines in the plane represent the continuations in λ keeping α fixed. We now represent the branch points by black squares and show the branches of buckled equilibria emanating from each of them. The vertices of the triangulation of the sheet are shown as circles on the branches. This triangulation is indicated by the dotted lines, although, for clarity, we show only the triangulation between the first pair of branches.*

and $(\lambda_k^{i,j}, \alpha^i), (\lambda_k^{i,j+1}, \alpha^i), (\lambda_k^{i+1,j+1}, \alpha^{i+1})$ for $1 \le i \le N-1, 1 \le j \le M-1$, as shown in Figure 7.7.

This method for generating bifurcation surfaces is fairly intuitive, but it may not produce smooth results when the surfaces are complicated, such as in the case shown in the second column of Figure 7.4. Folds and sharp bends can be difficult to track smoothly, and, because the different one-dimensional branches are computed independently, the grid may become significantly more skewed than in the relatively regular cases shown in Figures 7.6 and 7.7. However, if the geometry of the surface is sufficiently simple, or if the discretization is made sufficiently fine, then the surface can be smoothly portrayed.

For example, we now give two examples of the computation of sheets of relatively simple buckled equilibria. First, we consider the region of the $\rho = 1$, $\gamma = 1$ plane of unbuckled equilibria highlighted in Figure 7.8, and then we show in Figure 7.9 two sheets of buckled equilibria branching from this region. Each sheet required approximately 6 hours of computation on a 700 MHz Pentium III Xeon and consisted of 40 MB of data. For each equilibrium, the index was calculated using a numerical implementation of the conjugate point technique discussed in section 2.2, and the surface is color coded by index with the color scheme from Figure 6.2. The first sheet contains portions of the slices appearing in column 1 of Figure 7.2, while the second sheet matches up with column 1 of Figure 7.4. On the first sheet, buckled solutions very close to the plane of unbuckled equilibria are stable (green) if α is sufficiently small but have index 1 (yellow) for larger values of α. Continuing further on the sheet, we see that the stable equilibria give way to index-1 equilibria as buckling continues. This pattern is repeated on the second sheet but with index-2 equilibria giving way to index-3 equilibria.

As a second example, we consider the region of the $\rho = \frac{3}{2}$, $\gamma = 1$ plane of unbuckled equilibria highlighted in Figure 7.10, and then we show in Figure 7.11 two sheets of buckled

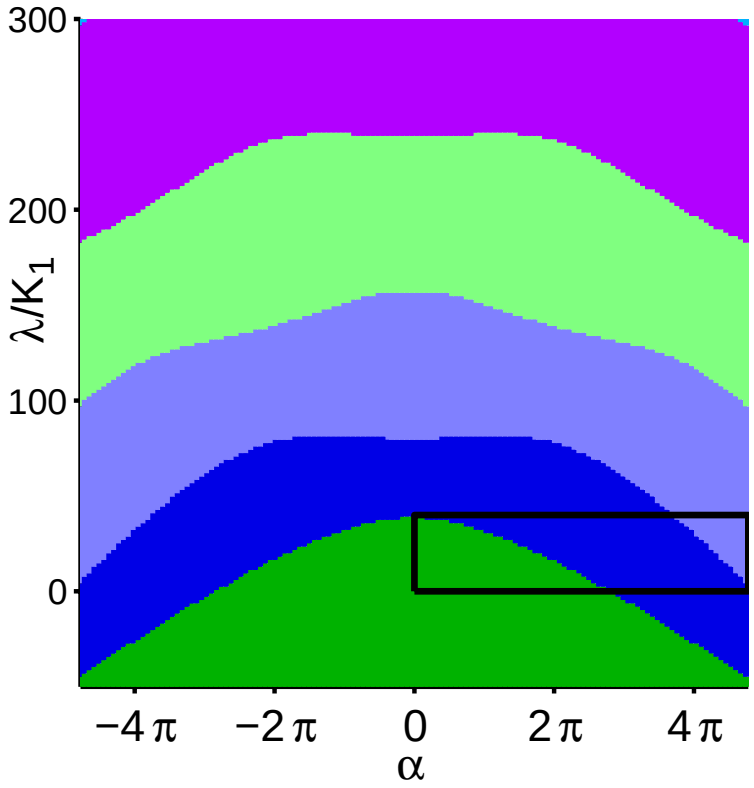

Figure 7.8. *A portion of the plane of unbuckled equilibria for an isotropic rod ($\rho = 1$) with twisting-to-bending stiffness ratio $\gamma = 1$. Within the region marked by the box, we will compute sheets bifurcating from the lines of color changes; these sheets are shown in Figure 7.9.*

equilibria branching from this region. In this case, the sheets of buckled equilibria match up with the slices appearing in column 2 of Figure 7.2, i.e., the splitting of the first sheet of buckled equilibria from the isotropic problem. The first sheet follows approximately the same pattern of index-0 equilibria giving way to index-1 equilibria that appeared in the isotropic case, while the second sheet involves a similar pattern of index-1 equilibria yielding to index-2 equilibria. This pattern is consistent with the usual expectation for stability of equilibria under symmetry-breaking perturbations: one of the perturbed images has the index of the symmetric case, and one has index one higher. In addition, we see a new feature in this case: the presence of a blue (index-2) patch on the first sheet. This blue patch exists because of a secondary bifurcating sheet, which is not shown in Figure 7.11 but can be clearly seen in the $(\alpha = \frac{3\pi}{2}, \rho = \frac{3}{2})$ slice in Figure 7.2 as a yellow dashed branch running on top of a solid blue branch. The solid blue branch is a slice of the blue patch in Figure 7.11, and thus we can infer that the blue patch is spanned by a nearly parallel yellow patch of which the yellow dashed branch is a slice. Looking through the slices in Figures 7.2 and 7.4, we can see that this is the simplest example of the type of surface branching and reconnection that proliferates through the bifurcation surface for more complicated buckled equilibria, not to mention the dependence of this topological structure on ρ and γ.

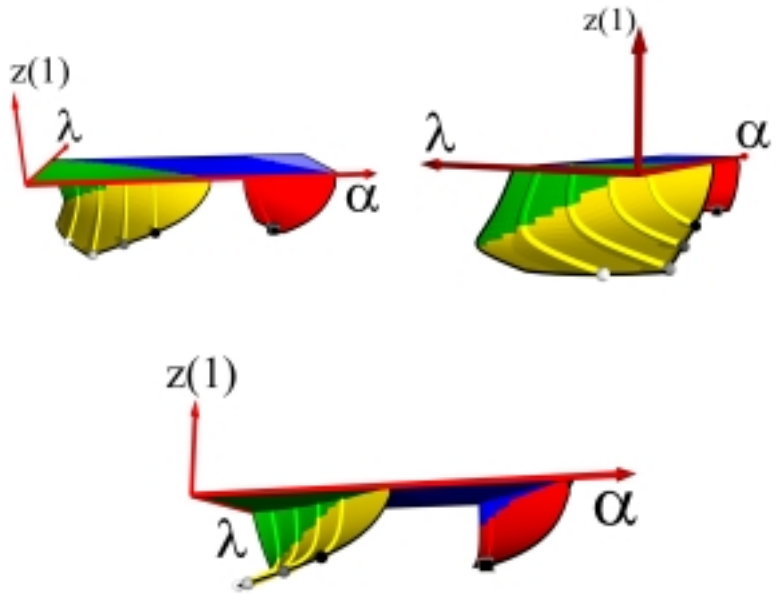

Figure 7.9. *Portion of the surface of buckled equilibria for an isotropic rod ($\rho = 1$) with twisting-to-bending stiffness ratio $\gamma = 1$, colored by the index of the equilibria according to the color scheme in Figure 6.2. For each buckled equilibrium, the value of the force λ, twist angle α, and length $z(1)$ are plotted, and three perspectives of the resulting surface are shown. The plane is the portion of the plane of unbuckled equilibria shown in Figure 7.8, and two sheets bifurcate from it. The origin of the red axes is at $(\alpha, \lambda, z(1)) = (0, 0, 1)$. The spheres and cube correspond to marked points in the left columns of Figures 7.2 and 7.4.*

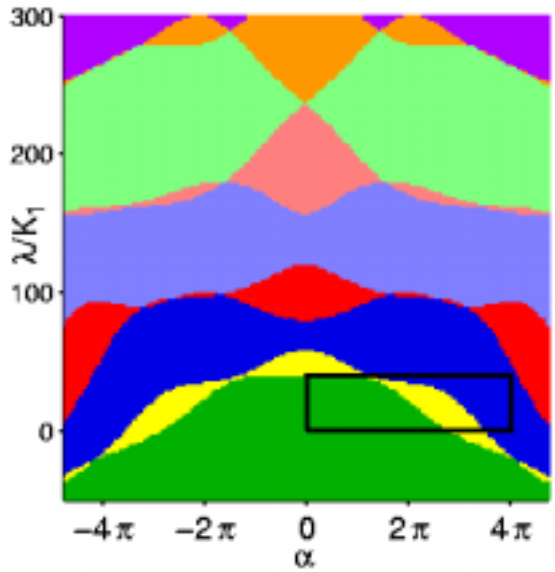

Figure 7.10. *A portion of the plane of unbuckled equilibria for $\rho = \frac{3}{2}$, $\gamma = 1$. Within the region marked by the box, we will compute sheets bifurcating from the lines of color changes; these sheets are shown in Figure 7.11.*

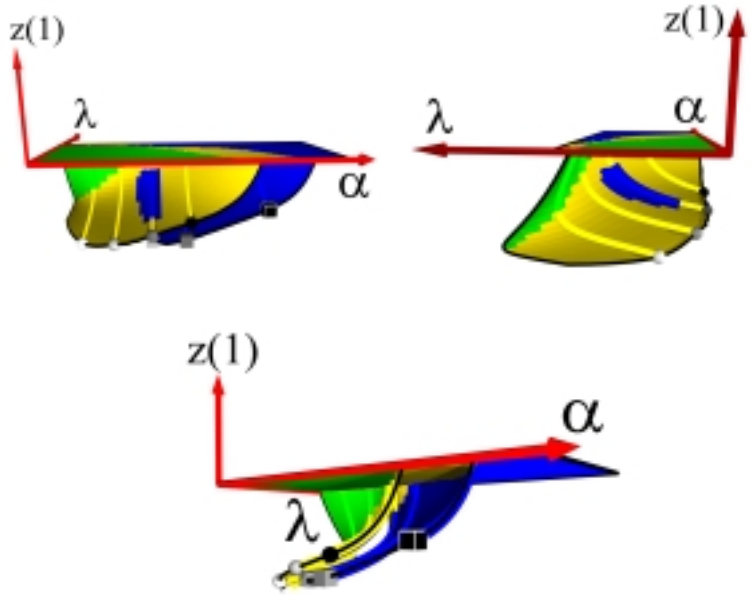

Figure 7.11. *Portion of the surface of buckled equilibria for $\rho = \frac{3}{2}$ and with twisting-to-bending stiffness ratio $\gamma = 1$, colored by the index of the equilibria according to the color scheme in Figure 6.2. As in Figure 7.9, three perspectives of the same surface are shown. The plane is the portion of the plane of unbuckled equilibria shown in Figure 7.10, and two sheets bifurcate from it. The origin of the red axes is at $(\alpha, \lambda, z(1)) = (0, 0, 1)$. The spheres and cubes correspond to marked points in the right column of Figure 7.2.*

8. Conclusions. In this article, we developed a significant simplification of the standard technique for determining the index of equilibria in parameter-dependent calculus of variations optimization problems. One might argue that in practice only local minima are of interest, in which case it would seem more efficient to employ a minimization algorithm directly rather than pursue the apparently circuitous strategy of finding all equilibria and then performing a conjugate point computation to locate the local minima. For a single optimization problem, this argument may be correct, but for a problem with one or more parameters, it is less clear. As the parameters are varied, the set of equilibria tend to form connected sets that are readily tracked by parameter continuation, as we have seen in the one-dimensional and two-dimensional bifurcation diagrams in this paper. In contrast, the local minima may exist in several disconnected regions of parameter space and hence may be more difficult to locate and track using standard minimization techniques.

Such computational issues aside, the equilibrium approach offers major advantages in terms of qualitative understanding. The differential equations describing equilibrium may yield to qualitative analysis, at least for a subset of the solutions, that leads to insight into the overall structure of the problem. The central result of this paper, the corollary in section 3 and its extension to isoperimetrically constrained problems in section 4, is an example of this type of analysis. This result applied to the unbuckled configurations of the elastic strut led to

a complete understanding of the stability index of these configurations, as shown in Figure 6.1. These unbuckled configurations were in turn the skeleton of the full set of equilibria, as seen in Figures 7.2, 7.4, 7.9, and 7.11, in that they provided the starting point for the numerical continuation necessary to compute the buckled configurations. As this pattern of complicated "nontrivial" solutions bifurcating from a "trivial" family of solutions is quite common, the combination of analysis and computation presented here could be applied to a variety of other parameter-dependent problems.

Acknowledgments. We thank John Maddocks for helpful discussions on some of these questions. Physical configurations and bifurcation surfaces were produced in POV-Ray.

REFERENCES

[1] S. S. Antman, *Nonlinear Problems of Elasticity*, Springer-Verlag, New York, 1995.
[2] O. Bolza, *Lectures on the Calculus of Variations*, 2nd ed., Chelsea, New York, 1961.
[3] A. R. Champneys and J. M. T. Thompson, *A multiplicity of localized buckling modes for twisted rod equations*, Proc. Roy. Soc. London A, 452 (1996), pp. 2467–2491.
[4] E. H. Dill, *Kirchhoff's theory of rods*, Arch. Hist. Exact Sci., 44 (1992), pp. 1–23.
[5] E. J. Doedel, H. B. Keller, and J. P. Kernévez, *Numerical analysis and control of bifurcation problems.* I. *Bifurcation in finite dimensions*, Internat. J. Bifur. Chaos Appl. Sci. Engrg., 1 (1991), pp. 493–520.
[6] E. J. Doedel, H. B. Keller, and J. P. Kernévez, *Numerical analysis and control of bifurcation problems.* II. *Bifurcation in infinite dimensions*, Internat. J. Bifur. Chaos Appl. Sci. Engrg., 1 (1991), pp. 745–772.
[7] G. M. Ewing, *Calculus of Variations with Applications*, Dover, New York, 1969.
[8] A. Friedman, *Foundations of Modern Analysis*, Holt, Rinehard, and Winston, New York, 1970.
[9] I. M. Gelfand and S. V. Fomin, *Calculus of Variations*, Prentice-Hall, Englewood Cliffs, NJ, 1963.
[10] A. Goriely, M. Nizette, and M. Tabor, *On the dynamics of elastic strips*, J. Nonlinear Sci., 11 (2001), pp. 3–45.
[11] A. G. Greenhill, Proc. Inst. Mech. Eng. (1883), p. 182.
[12] J. Gregory and C. Lin, *Constrained Optimization in the Calculus of Variations and Optimal Control Theory*, Van Nostrand Reinhold, New York, 1992.
[13] M. Gutzwiller, *Chaos in Classical and Quantum Mechanics*, Springer-Verlag, New York, 1990.
[14] M. R. Hestenes, *Calculus of Variations and Optimal Control Theory*, John Wiley and Sons, New York, 1966.
[15] H. B. Keller, *Numerical solution of bifurcation and nonlinear eigenvalue problems*, in Applications of Bifurcation Theory, P. H. Rabinowitz, ed., Academic Press, New York, 1977, pp. 359–384.
[16] G. Kirchhoff, *Über das Gleichgewicht und die Bewegung eines unendlich dünnen elastischen Stabes*, J. Reine Angew. Math., 56 (1859), pp. 285–313.
[17] A. E. H. Love, *A Treatise on the Mathematical Theory of Elasticity,* 4th ed., Dover, New York, 1927.
[18] J. H. Maddocks, R. S. Manning, R. C. Paffenroth, K. A. Rogers, and J. A. Warner, *Interactive computation, parameter continuation, and visualization*, Internat. J. Bifur. Chaos Appl. Sci. Engrg., 7 (1997), pp. 1699–1715.
[19] R. S. Manning, K. A. Rogers, and J. H. Maddocks, *Isoperimetric conjugate points with application to the stability of DNA minicircles*, Proc. Roy. Soc. London A, 454 (1998), pp. 3047–3074.
[20] M. Morse, *Introduction to Analysis in the Large*, 2nd ed., Institute for Advanced Study, Princeton, NJ, 1951.
[21] S. Neukirch and M. E. Henderson, *Classification of the Spatial Clamped Elastica,* I *and* II, preprint, available online from http://lcvmsun9.epfl.ch/~neukirch/publi.html.
[22] R. C. Paffenroth, *Mathematical Visualization, Parameter Continuation, and Steered Computations*, Ph.D. thesis, University of Maryland, College Park, MD, 1999.

[23] M. Renardy and R. Rogers, *An Introduction to Partial Differential Equations*, Texts Appl. Math. 13, Springer-Verlag, New York, 1993.
[24] H. Sagan, *Introduction to the Calculus of Variations*, Dover, New York, 1969.
[25] M. D. Schuster, *A survey of attitude representations*, J. Astronaut. Sci., 41 (1994), pp. 439–518.
[26] G. H. M. van der Heijden, S. Neukirch, V. G. A. Goss, and J. M. T. Thompson, *Instability and Self-Contact Phenomena in the Writhing of Clamped Rods*, preprint, available online from http://lcvmsun9.epfl.ch/~neukirch/publi.html.
[27] G. H. M. van der Heijden and J. M. T. Thompson, *Lock-on to tape-like behaviour in the torsional buckling of anisotropic rods*, Phys. D, 112 (1998), pp. 201–224.